FEASIBILITY STUDY OF GRID-CONNECTED HYBRID WIND-BATTERY ENERGY STORAGE SYSTEM FOR EV CHARGING STATION IN THAILAND

THUZAR MON

A THESIS SUBMITTED IN PARTIAL FULFILLMENT

OF THE REQUIREMENTS FOR THE DEGREE OF MASTER OF ENGINEERING

IN AUTOMOTIVE AND ADVANCED TRANSPORTATION ENGINEERING

SCHOOL OF ENGINEERING

KING MONGKUT'S INSTITUTE OF TECHNOLOGY LADKRABANG

YEAR 2023

KMITL-2023-EN-M-277-161

THESIS TITLE	Feasibility Study of Grid-Connected Hybrid Wind-Battery Energy Storage System for EV Charging Station in Thailand
STUDENT NAME	Ms. Thuzar Mon
STUDENT ID	63601190
DEGREE	Master of Engineering
PROGRAM	Automotive and Advanced Transportation Engineering
ADVISOR	Prof. Dr. Jarruwat Charoensuk
CO-ADVISOR	Prof. Dr. Katsunori Hanamura

ABSTRACT

This study presents a feasibility study and an optimization analysis for a grid-connected hybrid wind-battery energy storage energy system using Thai wind data. An EV charging station is incorporated. The investigations include wind data analysis using Weibull distribution, investigation of wind turbine performance, wind power modeling, and modeling of a battery energy storage system (BESS) of the EV charging station. The main objective is to minimize the loss power supply probability (LPSP) and obtain the least optimal levelized cost of electricity (LCOE) while maintaining reliable power supply for an EV charging station. The optimization of proposed hybrid energy system is performed using Artificial Bee Colony (ABC) algorithm, which balances reliability and economy of power system. The power exchange between utility grid and system components is ensured by the maximum energy amount of purchased and sold capacity to the grid. An economic analysis is performed based on different wind energy availability and sizing of battery energy storage system. Moreover, sensitivity analysis is conducted on the key parameters of system such as maximum grid purchased and sold capacity, wind speed, and battery sizing. Based on the results, the proposed system can be determined to be cost-effective and technically reliable hybrid power supply system to reduce the reliance on the utility grid.

Keywords: Grid-connected wind-battery energy system, Feasibility, Optimization, EV charging station, Levelized cost of electricity, Loss of power supply probability

ACKNOWLEDGEMENT

This study was completed according to the framework of Thailand Advanced Institute of Science and Technology and Tokyo Institute of Technology (TAIST-Tokyo Tech) program and was fully supported by National Science and Technology Development Agency (NSTDA), which I am sincerely thankful for giving me the opportunity to conduct this research.

I, gratefully acknowledge to my co-advisor Prof. Dr. Jarruwat Charoensuk of King Mongkut's Institute of Technology Ladkrabang and co-advisor Prof. Dr. Katsunori Hanamura of Tokyo Institute of Technology for their support and help throughout this study.

I would like to express my sincere gratitude to my advisor, Dr. Supakit Worasinchai of National Metal and Materials Technology Centre (MTEC), who accepted me as his research student in the first place, patiently continued to instruct and support me offering knowledge, advice, and encouragement over the years. This work would not have been possible without his guidance and understanding.

I am indebted to Dr.-Ing. Manop Masomtob and all the seniors of MP144 laboratory for many helpful suggestions and support for this work and I am thankful for the great foundation that I gained from all the teachers and instructors at the early stages of my study.

Lastly, I am forever grateful to have my family and friends for their unconditional love, support and for believing in me in every way I choose to walk. I also would like to compliment myself for not giving up on this journey and managing to take up all the experiences to the last.

Thuzar Mon

TABLE OF CONTENTS

LIST OF TABLES

LIST OF FIGURES

LIST OF DEFINITIONS

ABC	Artificial bee colony
AC	Alternative current
ACS	Annualized cost of system
BESS	Battery energy storage system
BEV	Battery electric vehicle
CFD	Computational fluid dynamics
DC	Direct current
EECMs	Equivalent electric circuit models
ESS	Energy storage system
EVs	Electric vehicles
HAWT	Horizontal axis wind turbine
HEV	Hybrid electric vehicle
HREs	Hybrid renewable energy systems
LA	Level of autonomy
LCOE	Levelized cost of electricity
LES	Large eddy simulation
LLP	Loss of load probability
LPSP	Loss of power supply probability
LTO	Lithium Titanate (Li2TiO3)
NACA	National advisory committee for aeronautics
NCA	Lithium Nickel Cobalt Aluminum Oxide (LiNiCoAlO2)

NMSE	Normalized mean square error
NPC	Net present cost
OCV	Open circuit voltage
PHEV	Plug-in hybrid electric vehicle
RC	Resistor-capacitor circuit
SOC	State of charge
SST	Shear stress transport
VAWT	Vertical axis wind turbine

CHAPTER 1

INTRODUCTION

1.1 Research Background

The Environmental crisis and depletion of fossil fuels have become increasingly recognized in recent years [1]. The use of the traditional fuel vehicles continuously causes a large amount of carbon emissions, and the environmental concern is becoming rapidly severe. In order to reduce carbon emission, both public and private sectors might need to pay attention to the investment of clean energy technology.

During the past ten years, electric vehicles (EVs) have become widespread because of their negligible gas emissions and less dependency on fossil fuels [2]. However, the employment of the EVs in the specific area leads to a charging station that has power to supply the EVs. One solution that might be possible and has been proposed is to integrate renewable energy sources to generate power into the EV charging infrastructure. According to the survey of world energy organization in 2020, as presented in Figure 1.1, the solar, wind, and bioenergy contributed up to 30%, 27%, and 12%, respectively, to the world power generation.

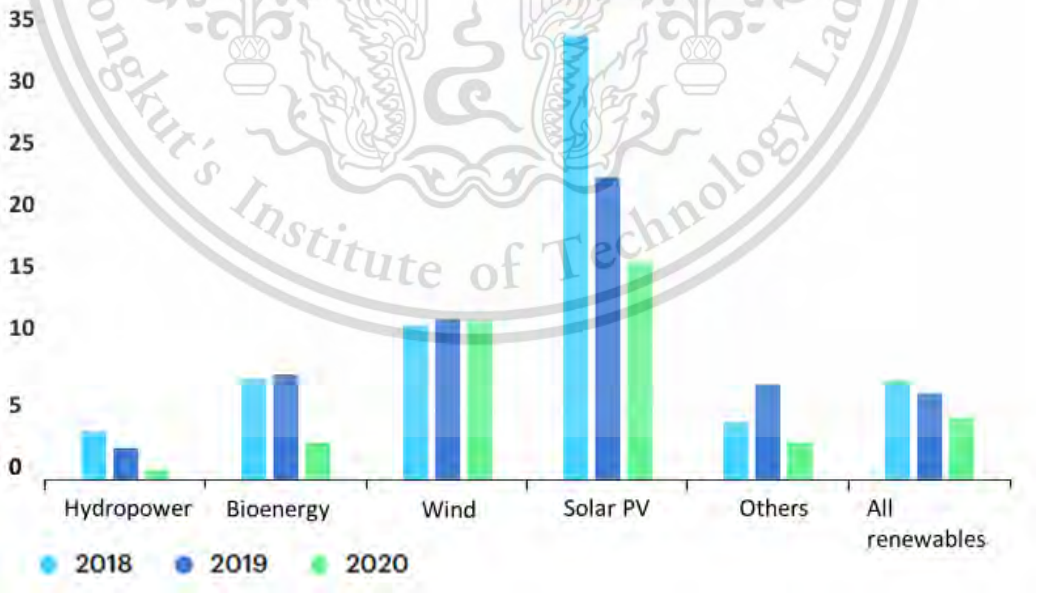

Figure 1.1 Annual growth for renewable electricity generation by source, 2018-2020

Source: IEA, Annual growth for renewable electricity generation by source, 2018-2020, IEA, Paris https://www.iea.org/data-and-statistics/charts/annual-growth-for-renewable-electricity-generation-by-source-2018-2020, IEA. License: CC BY 4.0

It can be observed that half of world power generation is provided by wind and solar power, suggesting that a promising large amount of power can be produced using these two sources of energy. In comparison, the use of wind turbines emits less carbon dioxide into the atmosphere. As presented in Figure 1.2, electricity production by wind power has rapidly increased by the support of research and development section. According to International Renewable Energy Agency (IRENA), the capacity of globally installed wind generation has expanded by a factor of 98 in the past two decades.

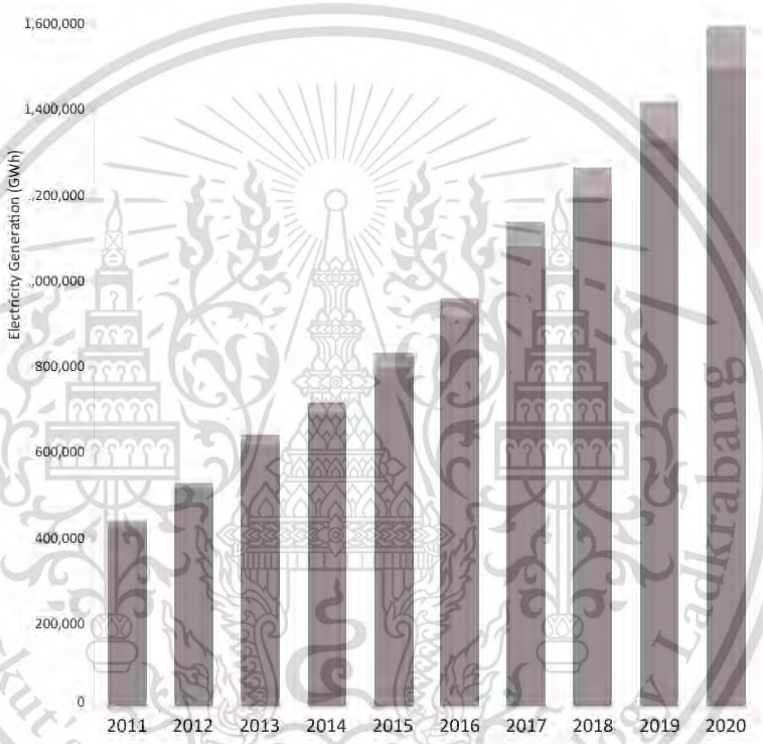

Figure 1.2 Wind power electricity generation trends

Source: https://www.irena.org/Energy-Transition/Technology/Wind-energy

Nevertheless, the wind power is not only intermittent but also low in the urban area. The power generated in this situation can be significantly varied and it is not known whether it will be able to produce power to supply to the EV charging station or not. Moreover, using wind electricity requires predictable and controllable energy storage system to supply stable power, i.e., battery energy storage system, into the electricity system. Integrating wind energy and battery storage system can be enhanced by an optimization method to investigate the system feasibility. This thesis will quantify it.

1.2 Research Objectives

The main objective of this thesis is to study the feasibility of techno-economic assessment for a grid-connected Wind-BESS energy system to supply the electricity to the EVs under Thai wind data.

1.3 Scope of Work

To achieve the above objective, this study will comprise of three main parts as follows.

1) wind turbine performance characteristics investigation
2) battery energy storage system modeling and
3) the overall energy system feasibility analysis and optimization.

1.4 Excepted Benefits

This study is expected to provide the following benefits.

1) Providing information for selecting small scale vertical axis wind turbine for the urban areas.
2) Providing potential insights into economic viability and suitability of Wind-BESS system in achieving cost-effective solutions.

1.5 Thesis Layout

This thesis is presented in five chapters as follows.

Chapter 1. Introduction: presents the overview of this thesis, research background, scope of work and expected benefits.

Chapter 2. Literature review: reviews the relevant studies related to this study including the survey on the vertical axis wind turbines, battery energy storage system modelling information, and optimization techniques of hybrid renewable energy systems.

Chapter 3. Methodology: explains the theories and methods applied for each model and procedure.

Chapter 4. Results and Discussion: presents the results analysis of the proposed system. It includes performance analysis, economic analysis, and sensitivity analysis.

Chapter 5. Conclusion: the final chapter describes the conclusion and recommendations for the future work.

The following papers are some parts of this thesis that have been published.

1. T. Mon, J. Charoensuk, K. Hanamura and S. Worasinchai, "Feasibility Study of Harnessing an Urban Wind Turbine to Supply an Electric Motorbike in Thailand," 2022 International Electrical Engineering Congress (iEECON), Khon Kaen, Thailand, 2022, pp. 1-4, doi: 10.1109/iEECON53204.2022.9741568.

2. T. Mon and S. Worasinchai, "Effects of the- Rotor -C-onfiguration and the -Airfoil Shape on the Darrieus Wind Turbine Performance," 2021 13th International Conference on Information Technology and Electrical Engineering (ICITEE), Chiang Mai, Thailand, 2021, pp. 110-115, doi: 10.1109/ICITEE53064.2021.9611958.

3. T. Mon and S. Worasinchai, “Performance Modelling of the Darrieus Wind Turbine.” *E3S Web of Conferences* 302:01001. doi: 10.1051/e3sconf/202130201001.

CHAPTER 2

LITERATURE REVIEWS

2.1 Modern Vertical Axis Wind Turbines and Their Limitations

The vertical axis wind turbine (VAWT) can be divided into two main types according to the aerodynamic function of the rotor. It is characterized by the fact that the rotor captures wind power from the aerodynamic drag of the air acting on the rotor or the aerodynamic lift created by the air flow. The VAWT that uses drag type rotor is called Savonius turbine and the one that uses lift type rotor is called Darrieus turbine. Nowadays, Darrieus wind turbine has been considered as a potential development for low-speed condition due to their fundamental simple design that allows for the ground-level mechanical housing, gear box, generator, and electrical components. It also eliminates the need for a yaw system because it is accessible to all wind directions [3]. The Darrieus turbine has been modified to the simplicity of the manufacturing called H-rotor, as straight blades are constructed instead of curved blades. The straight blades are mounted and attached to the rotating axis by the struts as shown in Figure 2.1.

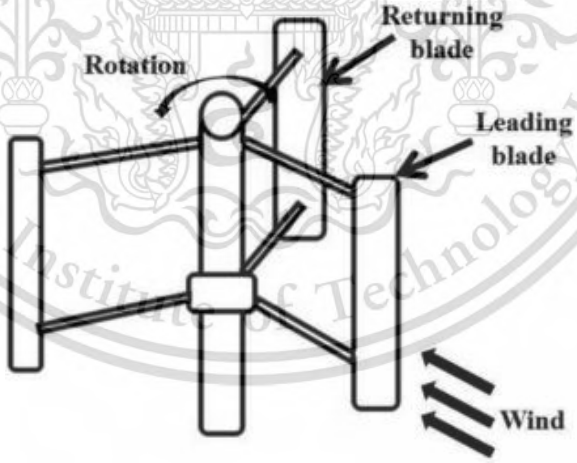

Figure 2.1 Three bladed H-rotor Darrieus wind turbine

Source: Sarathkumar Sebastin, J., Madhan Kumar, B., Shreedharan, M., Javadala, A.K., Manoj, V., Haribabu, C. (2023). Impact of Surface Roughness on the Aerodynamic and Aeroacoustic Performance of the Darrieus Wind Turbine. In: Natarajan, E., Vinodh, S., Rajkumar, V. (eds) Materials, Design and Manufacturing for Sustainable Environment. Lecture Notes in Mechanical Engineering. Springer, Singapore. https://doi.org/10.1007/978-981-19-3053-9_55

The US, the UK and particularly in Germany, several research improvements has been attempting to modify H-rotor turbine with the aim of reaching commercial maturity [4]. Nevertheless, this turbine design is not yet clear whether or not it will become a significant rival to the horizontal axis wind turbines (HAWTs). The basic advantages of this design also could prevail over its disadvantages. Therefore, the performance prediction of H-rotor turbine requires more investigations to outweigh its drawbacks such as low performance behaviors.

2.1.1 Small scale VAWTs

Numerous rotor designs are offered as market-ready commercial products based on the VAWT for use in urban applications. The 2.5 kW Turby turbine, [5] was developed by Delft University of Technology to be used in urban areas. To lessen the ripple torque operating on the bearing, its blades were twisted. Its height is slightly more than its diameter despite the twist., Figure 2.2(a). Similar rotor designs were the Quiet revolution, Figure 2.2 (b), [6], the VisionAir5, Figure 2.2 (c), and the Cleanfield turbine, Figure 2.2 (d). However, the Windspire turbine has a rotor that is relatively tall, measuring 5.08 in height to diameter as shown in Figure 2.2 (e). Table I. summarizes specifications of these turbines [7].

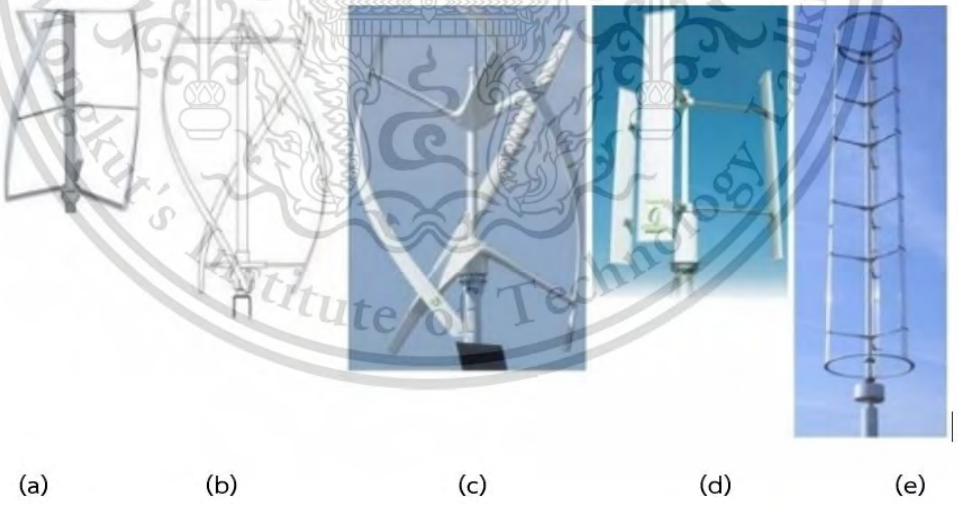

Figure 2.2 The Darrieus turbines for urban applications: (a) Turby (b) Quiet revolution (c) VisionAir5 (d) Cleanfield (e) Windspire

Source: VisionAir 5 - V-Air (visionairwind.com) , https://verticalwindturbineinfo.com/vawt-manufacturers/cleanfield-energy/

Table 2.1 Urban rotor configurations of the Darrieus wind turbine

Rotor type	Parameters			
	Airfoil	Chord length (m)	Height (m)	Diameter (m)
Turby	NACA0018	0.1	2.65	2.0
Quiet revolution	NACA – Symmetrical series	0.32	5.5	3.1
VisionAir5	NACA – Asymmetrical series	0.55	5.2	3.2
Cleanfield	NACA0021	0.40	3.11	2.75
Windspire	DU-06-W-200	0.15	6.1	1.2

2.1.2 Sensitive factors on VAWTs performance

Although the market for manufacturing Darrieus wind turbines shows a great demand, the performance of VAWTs is affected by many factors, particularly choosing the right airfoil, the rotor configuration and solidity. All of those factors make choosing the suitable airfoil more challenging. Most frequently, numerical fluid dynamics methods are used to select airfoils before the employment to the experimental work. Performance investigations on Darrieus wind turbine has been studied in the accountable number of previous studies. A series of numerical simulations had conducted to study the effects of the airfoil sections on the turbine performance [8]. The airfoils investigated were the conventional 4-digit NACA series. By changing the thickness and camber of the airfoil form, the impact of thickness and camber was investigated. The thickness under investigation ranged from 12 to 21 %, while the camber values were between 1 and 4 %. It has been demonstrated that % is the ideal thickness value, and that a 1% increase in camber can increase power output even more. Power production dropped as the camber angle increased further. The investigations of the S-series airfoils in comparison with the conventional NACA0018 section was performed in [9], [10]. It was revealed that the S1046 airfoil outperforms

the conventional sections. Experimental and computational research were provided by [11] to assess the aerodynamic performance of a small-scale Darrieus type straight bladed vertical axis wind turbine. That work investigated a few design characteristics including the blade number, the sectional profile of airfoil and the solidity effect. According to the laboratory tests and numerical calculation, the optimum design has an ideal power coefficient which is equal to 0.32 and 0.36 at a tip speed ratio of 3.4, respectively.

Despite the fact that VAWTs have a number of advantages over HAWTs such as its blades are easy to fabricate and provide a good opportunity for cost reduction, there is no reliable research whether how the rotor should be designed to improve the turbine performance which is one main drawback of VAWTs in comparison with HAWTs [12].

Furthermore, the solidity effect is an important index to judge the aerodynamic performance of wind turbines as it is closely related to the utilization rate of wind power. Therefore, the design of solidity is also critical to investigate. Solidity is defined by three factors: blade number, chord length, and rotational radius of turbine. A more comprehensive study for the influence of solidity on H-VAWT aerodynamic performance can be evaluated by varying those factors. The maximum power coefficient will be obtained within low tip speed ratio of high solidity, while it will drop to low solidity of H-VAWT. Nevertheless, the paper makes note of the fact that, despite having the same solidity, the performance of H-VAWT will be significantly altered by various combining configurations of the chord length and the blade number [13].

The numerical investigation for different solidity was implemented in [14] and as the results show, changing the radius and the number of blades has practically identical impacts on turbine performance. On the other hand, changing the chord length can increase the peak value of power coefficient, while the increase of blade number decreases the peak value of power coefficient.

2.1.3 Estimation of wind energy potential

Regardless of the fact that there is a growing interest in wind energy, its uncertainty makes wind energy the most challenging and important aspect of wind

energy development. Generally, the estimations of wind potential in the literature were made by examining the wind data. Numerous studies have been conducted to analyze the viability of wind energy at particular sites. There are two types of wind power forecast methods: physical and statistical. The physical method implies physical considerations such as terrains, topography, local pressure, and temperature to predict the energy potential. The statistical method employs statistical models to establish the relationship between wind power potential and other parameters along with historical and future forecasted values. Regarding the significant of determining wind potential, it is acknowledged that measured data is considered to be the best for assessment. Satellite wind data might be utilized as an alternative in the areas where year-long time series data is not available. A pre-feasibility wind potential study is conducted in Yulchon district of South Korea using averaged wind data for 1 hour at 10m height in order to investigate the wind farms with different wind turbines [15]. In [16], a study of wind data is presented at 17 different sites on all of territory of Tunisia to develop a database for the wind power users. They described wind characteristics by using wind charts to categorize with the most, average, and low wind potential. In comparison with other models, Weibull distribution offers a better fit to probability distributions of wind speed data by using statistical methods [17]. A several probability distribution functions of different wind regimes [18] were reviewed to make a comparison between those models and concluded that the two parameter Weibull distribution is the most flexible and applicable over the complete range of wind speed. A method of fitting low wind speed data to Weibull distribution is presented to prove that the entire range of wind speed data can be filled into the two-parameter Weibull distribution if the anemometer used has sufficient resolution [19].

2.2 Integration of Wind Energy into EV Charging

As electricity generation using wind power has received considerable attention worldwide in recent years, there are particular issues that need further study and research. In order to maintain the quality of supplied power, smoothing fluctuation of wind power output and determining the storage capacity are required to be addressed. To address such problems, integrating renewable sources especially wind power generation or solar power generation systems with energy storage system (ESS) is one

promising way to approach. Given the rapid development of batteries, the BESS can be used to regulate the output variations of renewable energy sources like solar and wind. Furthermore, the above-mentioned hybrid power generation system can have its power quality improved by integrating a BESS in the system.

The effectiveness of wind energy generation system to power an EV charging station using simulated hourly wind distributions in [20] demonstrated to deliver accurate estimations. The accurate estimations included both wind power stability across short time intervals and the capacity of EV charging station. The installation of wind, PV power generation and energy storage system to EV charging station can help to balance the electricity supply and demand by lowering environmental pollution, costs, and influence of utility grid. In [21], an EV charging station is constructed employing wind, solar and ESS systems to forecast EV load demand and determine how to configure the maximum capacity of system components. The major drawback is the high-power demand if a charging station is considered to be fast charging station. Even if incorporating renewable energy sources might boost charging station profitability, it is necessary to connect them to the grid or equip them with a storage system to counteract the intermittent nature of renewable energy. Though the expensive investment, there is a tendency in technological advancement toward cost reductions, which is an especially intriguing factor in determination of batteries, storage systems and electric vehicles leading this perspective to support decentralized generation for more sustainable energy management.

Moreover, there is another type of wind powered EV charging station considering vehicle to gird technology [22], called a novel-gird connected power system. It consists of wind energy conversion system connected with a unidirectional DC/DC converter, a maximum power point tracking (MPPT) controller, bidirectional DC/DC converters equipped with charging stations and a three-phase bidirectional DC/AC inverter connected to the gird. The experimental verifications in the novel-grid connected system demonstrated that the built EV charging station may help the local power distribution system, particularly when load demand is at its highest, in addition to supplying energy to charge EVs.

The reliability of a wind-powered system with a high wind energy penetration rate is not at risk as a result of high wind power penetration because the problem can

be fixed by changing the turbine blades [23]. The issue of excessive electricity production in Denmark's areas with high wind penetration could have been configured. However, the issue of too much wind is as challenging to manage as the issue of insufficient wind. Excess wind implies that the system is not able to achieve the optimal economic payback for the wind capacity investment and to minimize the emissions.

2.3 Estimation Methods of EV Charging Station Capacity

Estimating the EV charging load is the foundation for designing the entire system. Many academics have conducted critical research on EV charging load prediction and provided noteworthy findings. According to the existing research, there are four techniques: the constant method, the behavioral analysis method, the simulation method, and statistical analysis technique.

The charging methods used by various charging stations in the remote areas of the Democratic Republic of the Congo [24] were investigated, based on the assumption that the charging load at the charging stations is constant. In that study, the power flow from renewable energy sources toward electric vehicles through DC bus is composed, taking into account PV and wind with battery storage system. When the charging load is set as a constant for the wind-powered grid-connected EV charging station on an on-shore location. the load demand can be estimated based on the statistical research on daily electric power demand around the location of charging station [25].

Behavioral analysis is known as building a model that represents how EV users typically travel in a particular location and over a given period in order to determine the charging load. Travel chains and traffic matrices are commonly applied in behavioral techniques to represent the real condition and presented hypotheses. The relationship between EV charging station architecture and charging probability can be computed using a heuristic method to predict the charging probability [26].

Simulation method is a technique to address the inconsistent character of EV charging behavior. The frequently used simulations are MC simulation and random simulation. MC simulation is used to analyze the travel habits of EV users and three

key aspects of EV charging, including starting level of charge, charging start time, and EV charging characteristics, to predict the load [27].

2.4 State of Charge Calculation Methods

The various mathematical SOC estimate techniques are divided into categories based on approached methodology. According to the pertaining literature, [28], [29], SOC estimation methods can be classified into four main categories as follows.

1) Direct measurement: The direct measurement methods are referenced by battery physical characteristics such as terminal voltage and impedance.
2) Book-keeping estimation: The book-keeping methods use the discharging current as an input and integrate it over the time period.
3) Adaptive systems: The adaptive methods automatically modify the SoC for various discharge situations. The most common methods used are the fuzzy neural network method and Kalman filter method.
4) Hybrid methods: The hybrid methods combine the capabilities of each SOC estimation method to offer a substantially optimal estimation performance.

The applications of particular SOC estimation techniques for battery management system can be specifically varied. Table 2.2 shows the categorization of SOC estimation methods in the existing literature.

Table 2.2 Classification of SOC estimation methods

Category	Methods
Direct measurement	Open circuit voltage method
	Terminal voltage method
	Impedance method
Book-keeping estimation	Coulomb counting method
Adaptive systems	Fuzzy neutral network
	Kalman filter
Hybrid methods	Coulomb counting and Kalman filter combination
	Coulomb counting and EMF combination

A variety of battery models with different levels of accuracy and complexity have been developed over the years [30]. There are typically three different types of battery models: the electrochemical model, the reduced-order model, the equivalent electric circuit models (EECMs), and the neural network model. These types are determined by the level of physical interpretation of the battery electrochemical processes in the model. Precise parameter identifications are essential for accurate predictions of any state of a battery. For lithium-ion batteries, open circuit voltage (OCV) is an important characteristic to estimate SOC. In order to obtain a great significance of lithium-ion battery management, the OCV value of corresponding SOC is important [31]. To observe the dynamic behavior of the battery, it has been suggested to use a linear structure made up of an ideal voltage that represents the open circuit voltage (OCV), which is regulated by SOC and temperature, a resistor that stands in for internal resistance, and some resistor-capacitor (RC) circuits. The accuracy of this model is not only adequate for most system applications but also the particular battery chemistry is not required, that reveals it can be used with different battery kinds.

2.4.1 Open circuit voltage

The OCV is fundamental for developing electric models of batteries. The OCV as a function of SOC dependency is used in an attempt to model and predict the behavior of battery. An OCV-SOC curve can be derived from the experiments and applied to the battery model either as a lookup table or an analytical expression. Nevertheless, expressing the OCV-SOC curve as an analytical function is vulnerable to inaccurate estimation [32]. Consequently, it is decided to use the OCV-SOC curve as a lookup table in battery modeling. The OCV and SOC relationship could not exactly be the same for all battery types. For lead-acid batteries, the relationship between the SOC and its OCV is approximately linear in contrast to lithium-ion battery, which is used in this study. A typical relationship between SOC and OCV in lithium-ion battery is shown Figure 2.3.

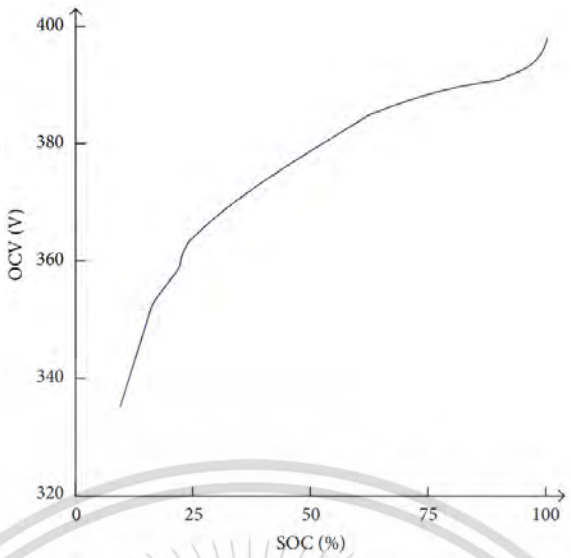

Figure 2.3 A typical relationship between SOC and OCV of lithium-ion battery

Source: Dong Tingting, Li Jun, Zhao Fuquan, You Yi and Jin Qiqian, "Analysis on the influence of measurement error on state of charge estimation of LiFePO4 power Battery," 2011 International Conference on Materials for Renewable Energy & Environment, 2011, pp. 644-649, doi: 10.1109/ICMREE.2011.5930893.

2.4.2 Internal resistance

To determine energy efficiency and heat evolution of battery under high current loads, the interior resistance or internal resistance is primarily used for a given battery voltage as Overpotential resistance is the principal reason of heat emission in batteries. The voltage of battery cell under load is influenced by the OCV as well as the voltage drop caused by interior ohmic resistance [33]. When measuring resistance, the testing device is either given a voltage, and the corresponding current is measured, or a current is applied, and the voltage produced is measured.

2.5 Optimization of HREs Power System

Hybrid renewable energy systems (HREs) can be managed to operate as both stand-alone and grid connected systems. The performance and reliability of these systems depend on the optimization of design and effective unit sizing of components. Optimization is a method to determine the sizings of a system by balancing the system cost and the system reliability while meeting the load demand of the system.

The literature study indicates that the methodologies for the optimal design of HREs have been generally established as multi-objective and single objective according

to purpose of desired system. The objectives can be justified numerically or analytically by using different algorithms and operation strategies. The most frequently used function in a variety of single objective systems is the overall cost of the system. [34], such as annualized cost of system (ACS), net present cost (NPC), and levelized cost of electricity (LCOE).

2.5.1 Indicators of HRE power system optimization

The decision of optimization objectives significantly affects the outcome of considered system configuration. In existing research, the problems of objective optimization are primarily associated with economic indicators, reliability indicators and environmental indicators. The indicators applied to evaluate the optimization objectives and constraints provide a framework for the building mathematical model.

2.5.1.1. Economic indicators

The system's economic feasibility is determined using economic indicators. The economic or cost indicators can be classified as follows:

Total Annualized Cost of System (ACS) consists of the annual investment cost, replacement cost, and maintenance cost.

Levelized Cost of Energy (LCOE) is a fixed price per unit of electricity generated over a given time period. LCOE is denoted as the ratio of the total annual expense to the total annual power supplied by the system.

Net Present Cost (NPC) is one of the most popular financial tools for determining a project's economic viability. The NPC of an investment is the difference between its current worth and its cost of expense over the entire lifetime.

2.5.1.2. Feasibility indicators

Indicators of feasibility are used to measure the capability of a system to meet the load demand continuously and effectively. The most commonly used feasibility indicators are as follows:

Loss of Power Supply Probability (LPSP) describes the ratio of total energy that shortfalls to the load demand over a time.

Expected Energy not Supplied (EENS) is a probabilistic indicator that quantifies the anticipated energy demand that the system won't be able to meet due to a lack of available capacity.

Level of Autonomy (LA) defines the proportion of the total operating hours and the total hours during which there are no load losses.

2.5.2 Evaluation techniques of optimization methodology

The study indicates that there are two evaluation methods to investigate feasibility indicators; deterministic methods: it assumes that the demand load, energy sources especially PV panels and wind speed behaviors are constant over a period. A mathematical model is used to describe the indicator. A huge data set for the considered period is used as an input in order to make sure optimum performance [35].

Stochastic methods: these techniques create appropriate models to predict the system's output while taking into account the unpredictable behavior of the input data, such as wind speed, solar irradiance, and demand. Simulation approaches are used to determine those input data and probabilistic methods can be applied adjust probability distributions of the input variable behaviors before integrating them to compute the system output [36]. The methodology and system configuration can be designed according to the proposed objective problems and constraints.

The determination of optimal sizings of a micro-grid connected system is implemented in [37] through minimizing the discrepancy between the power production and consumption characteristics by scheduling of dispatchable loads using HOMER software. That work investigated how demand response usage affects the loss of generated energy by comparing the results of with and without demand response. The conclusion indicated that implementing a demand response program lowered the quantity of batteries, inverters, and hence the net present cost (NPC) of system.

A mathematical model developed in [38] to optimize a hybrid solar-wind energy system with a battery energy storage system for a remote island area used genetic algorithm (GA). The results were compared for four different separate cases. In this research, two different wind turbine sizes were also analyzed, suggesting that the size of wind turbine has an impact on the reliability of the system. As optimization objectives, the performance of system with effects of loss of power supply probability (LPSP), deviations of renewable energy sources on the feasibility of system were analyzed.

A hybrid wind-PV system is a viable alternative to reduce the rising energy demand [39]. Nevertheless, a reliability indicator named maxENS was proposed to be used as a probabilistic technique to calculate the degree of reliability due to high unpredictability and uncertainty of renewable energy. Utilizing the simulated annealing (SA) technique, research was conducted on a PV/wind energy generation system in Turkey with the goal of maximizing system capacity while reducing system costs [40]. The size of the PV, the swept area of the wind turbine rotor, and the battery capacity are the key variables.

A multi-objective optimization model [41] proposed for the hybrid energy storage system of non-grid-connected wind power and energy storage with a genetic algorithm. Two decision variables; the amount of batteries and supercapacitors were taken into consideration based on the aim of maximizing annual profit and minimizing wind constraints. In addition to solar and wind energy connected to grid, integrating with diesel generators are also potential energy supply system, [42], it is crucial to determine the size of system, cost, and technical feasibility for present and future use. This paper studied optimization approach to observe the loss of power supply probability (LPSP), cost of electricity (COE), and renewable factor of hybrid micro grid system components regarding to overall reliability of system.

A description of a new methodology for optimizing renewable energy systems employs the Normalized Weighted Constrained Multi-Objective Optimization algorithm (NWCMO) [43]. It provides to find an agreement between conflicting technical, economic, environmental, and sociopolitical goals, which included indicators such as levelized cost of electricity (LCOE), socio-political index (LPSP) and values of carbon emissions.

A nonlinear constraint multi-objective optimization can be implemented using fuzzy self-adaptive particle swarm optimization (FSAPSO) [44]. This optimization method dispatches the consideration of economics and emission as primary competitive objectives to reduce the overall cost while simultaneously taking environmental concerns into account.

A photovoltaic-wind-hydropower system was studied as a case study in China by using techno-economic index [45], which attempts to obtain the optimum configuration with the highest level of feasibility for power supply and lowest possible investment cost such as LPSP, COE and other indicators. This study performed a comparative study using Particle Swarm Optimization (PSO), genetic algorithm (GA), and Simulated Annealing (SA) algorithm. Moreover, this work analyzed the impact of wind curtailment rate on the objectives of system and provided various potential results.

A techno-economic study of a grid connected solar-fuel cell energy system as presented in [46] considered the costs of energy purchased and sold to the grid. The net present cost (NPC) was optimized by using three algorithms, namely, artificial bee colony (ABC), particle swarm optimization (PSO) and a hybrid of ABC and PSO.

In the optimization strategies of HREs, it requires to optimize the schedule of system operation. Augmented non-dominated constraint method (ANEC) is promising to use to propose an optimization model for scheduling EV charging and discharging [47]. It considers battery degradation, end user energy cost, grid net change and carbon emissions while providing frequency regulation. The research on capacity configuration optimization in this study is summarized in Table 2.3.

Table 2.3 Summary of survey on different configurations of HREs optimization

Reference	System component	Objective
[34]	Wind/PV/BESS	LCOE, NPC, ACS
[36]	PV/Wind/Diesel	NPC
[37]	PV/Wind/BESS	NPC
[38]	PV/Wind/BESS	COE
[39]	Wind/Solar	maxENS
[40]	Wind/PV/Battery	Total cost
[41]	Wind/Supercapacitors/Battery	Wind curtailment rate, Annual profit
[42]	PV/Wind/Diesel	LPSP, COE
[43]	PV/Wind/BESS	LPSP, LCOE
[44]	Wind/PV/Battery/Fuel cell/Micro-turbine	Total cost, Carbon emission
[45]	Wind/PV/Hydro power	COE, LPSP
[46]	PV/Fuel cell	NPC

CHAPTER 3
RESEARCH METHODOLOGY

This study focuses on the feasibility of the grid-connected wind-BESS energy system for an EV charging station under Thai wind data. To achieve that, a number of investigations have to be performed. The investigations are the modeling of wind data, the modeling of the wind turbine performance, and the modeling of the battery system. All of these models are used to optimize the feasibility of the proposed power system. This chapter presents the details of all the modeling techniques and optimization of the proposed grid- connected HREs.

3.1 The Wind Energy

Wind power is greatly influenced by geometry and although there are powerful winds in many places across the world, the considerable fine locations are significantly selective. In this context, decentralization can play a potential role in creating a cost-effective, reliable, and clean electricity system for locations such urban areas where strong wind speed is not accessible. Decentralized systems are extensively emphasized in transition scenarios which lead to a clean and effective energy future. The decentralized system enables the generation of renewable energy sources, which are dispersed and mainly supported by installations of small-scale technologies. The idea of decentralization wind energy and small-scale technology, has the extensive potential not only to provide the domestic power demand but also to support such as grid-connected systems in order to assess the suitability and economic viability of hybrid power generation.

Vertical axis wind turbines (VAWT) and horizontal axis wind turbines are the two main categories of wind turbines used to harness the wind (HAWT). Since HAWTs are known to be more efficient than VAWTs in steady winds, they have been utilized in large-scale wind farms for quite a long time. In contrast, VAWTs outperform HAWTs in the locations where the available wind speed is low and turbulent [48]. The most significant factor to choose VAWT over HAWT for the above-mentioned areas, is VATWs are able to function in the multidirectional flow to respond instant changes in wind

speed and direction in residential areas, which make VAWTs more efficient in turbulent wind flow. Nonetheless, it is critical to evaluate wind potential of selected location and turbine performance according to specific power curve prior to implementation of wind power in the considered power optimization system.

3.1.1 Wind Data Analysis

A wind turbine power curve and the wind speed distribution can be used to estimate the potential energy production for a particular wind turbine at a particular location. For visualizing the frequency of various wind speeds for a given place, a wind speed distribution created from measured data is a valuable tool. Weibull distribution is used in this section to estimate the power curve produced by the measured wind speed distribution.

The wind measurement was taken at Thailand's EGAT learning center in Bang Kruai. It was measured with an anemometer at a height of 6 meters and then logged to a data logger at a 1 second sampling rate. The frequency representation of this wind data was binned and analyzed accordingly.

It has been discovered that the two-parameter Weibull distribution offers an excellent fit with measured wind data to describe wind ranges. The following equation provides the probability density function.

$$f(v) = \frac{k}{c}\left(\frac{v}{c}\right)^{k-1} \exp\left(-\left(\frac{v}{c}\right)^{k}\right) \tag{3.1}$$

where:

v = the wind speed [m/s]

k = the Weibull shape factor [unitless]

c = the Weibull scale parameter [m/s]

The scale parameter, c, is the Weibull scale factor, a measurement of the wind speed distribution. The shape parameter, k, is the Weibull shape factor. It has a value between 1 and 3 and describes the appearance of a Weibull distribution. Very

fluctuating winds are denoted by a small number of k, whereas steady winds are denoted by a larger k. Additionally, the average wind speed increases as k increases. Modifications to the shape and scale parameters are made to further study the effect of wind characteristics on the overall energy output of the turbine and the results are discussed in Chapter 4.

3.2 The Vertical Axis Wind Turbine

The turbine investigated in this thesis is the straight-bladed vertical axis wind turbine. Figure 3.1 presents this type of turbine.

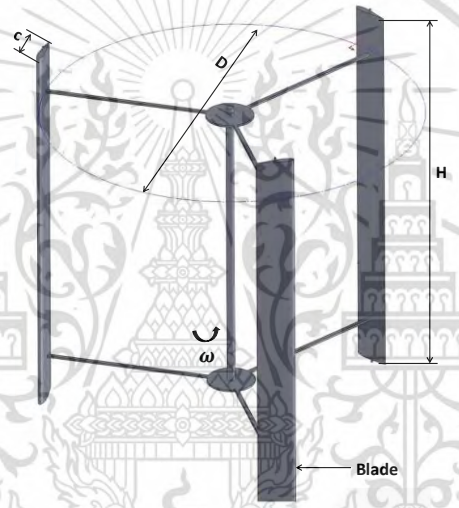

Figure 3.1 The straight-bladed vertical axis wind turbine

There are a number of parameters which affect the performance of VAWT. Amongst of all, solidity effect, rotor configuration, and airfoils are investigated in this study and the turbine performance is indicated by the power coefficient, C_p, also called the performance curve.

The performance curve depicts the power performance of wind turbine such as the maximum power coefficient with the corresponding optimal tip speed ratio at which the turbine blades are receiving optimal flow circumstances and extracting the optimum energy from the wind. The turbine efficiency decreases once the value of tip speed ratio is passed beyond the optimal value because of a barrier effect that prevents the wind from passing through the turbine. The coefficient of power and tip speed ratio of blade can be numerically expressed as follows.

$$C_p(\lambda) = \frac{P_w}{0.5\rho A V^3} \tag{3.2}$$

$$\lambda = \frac{\omega R}{V} \tag{3.3}$$

where:

P_w = the power generated by wind (W)

ρ = the air density (kg/m^3)

A = the swept area of turbine (m^2)

R = the rotor radius (m)

λ = the tip speed ratio of the blade

V = the wind speed (m/s)

Another parameter that influences the effectiveness of VAWTs is solidity. Solidity, σ, is the ratio of total rotor planform area to the total swept area. The different solidity investigations were made by changing the radius, R, and chord length, c, as it is defined as $\frac{Nc}{R}$. The maximum power coefficient and optimal tip speed ratio are profoundly influenced by solidity as shown in Figure 3.2. The description of solidity clarifies that as solidity increases, so will the mass of the turbine and the cost of production [49]. Therefore, solidity is considered to maximize turbine efficiency without consuming excessive material for rotor blades. The results of a computational fluid dynamics simulation for a H-type VAWT concluded that from the perspective of power generation, a high solidity is not recommended because of its poor efficiency and limited performance curve [50], [51].

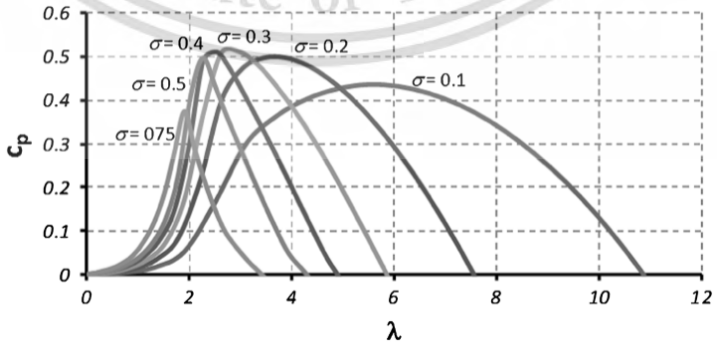

Figure 3.2 Effect of solidity on the power performance of VAWT

Source: Brusca, S., Lanzafame, R. & Messina, M. Design of a vertical-axis wind turbine: how the aspect ratio affects the turbine's performance. *Int J Energy Environ Eng* 5, 333–340 (2014). https://doi.org/10.1007/s40095-014-0129-x

On the other hand, exceedingly low solidities are unfavorable since they result in poor peak efficiency and high rotational speeds. Although there have been a number of studies on the solidity effect of H-type vertical axis wind turbines, the conclusions are still not generalizable, and the effects of radius and chord length on wind energy generation have not been considered in their entirety. Utilization rate of wind power is a crucial index to judge the aerodynamic performance of wind turbines, and as solidity is greatly related to utilization rate, the evaluation of solidity effect is important to optimize for wind power generation.

Performance of wind turbine is mainly dependent on the rotor configuration especially for the blade length and its position relative to the axis and the airfoils employed. The airfoil selection has a significant effect on the aerodynamic efficiency and structural integrity of each blade for the unstable functioning of VAWT with relatively changes of velocity. Early VAWT prototypes mostly made use of symmetrical NACA series from the aircraft industry. The 4-digit NACA airfoils, created by the National Advisory Committee for Aeronautics (NACA), describe the cross-sectional form of a wind turbine blade or the outline shape of an aircraft wing. There are two main types of airfoils widely used in the manufacturing of vertical axis wind turbines: symmetrical NACA series and S-series airfoils. The symmetrical NACA airfoils mainly depend on the thickness for the complete description [52]. Apart from the conventional NACA series, the use of S-series airfoils (S1012, S1016, S1046, S1048) become a promising improvement for the VAWTs efficiency [53].

In this study, the turbine investigated is a three-bladed vertical axis wind turbine with different rotor configurations. The first model is square and has the same width and height of 0.8 metre. The second model is rectangle and has the width and the height of 1.6 and 0.8 metre and the third model is cylinder with the width of 0.8 metre, the height of 1.6 metre. In order to distinguish the turbine models simpler, each turbine is labelled as D01 for the first turbine, D02 for the second turbine and D03 for the third turbine as displayed in Figure 3.3.

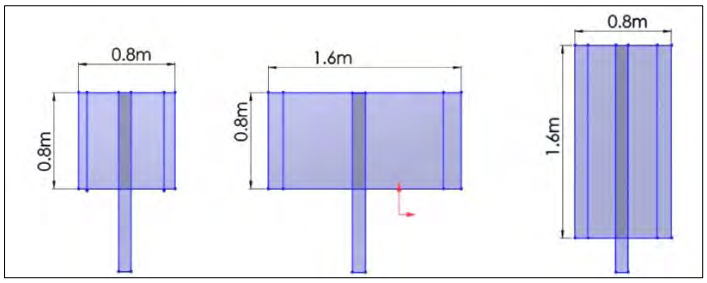

Figure 3.3 Rotor configurations

The NACA0021 and S1046 airfoils were examined. The NACA0021 section was chosen as a stand-in for the conventional NACA section. The S1046 was chosen because it has been shown in numerous studies to function well and to be a promising airfoil for this type of vertical axis wind turbine.

NACA0021 is a four-digit NACA number. It has a thickness of 21% which is located at the 30% of the chord. It was extensively used in the early development of the Darrieus turbine because it is symmetrical and can perform effectively when the turbine spins across its vertical axis, despite the fact that it was created for aircraft purposes.

The S1046 airfoil is a symmetrical, low-Reynolds number airfoil. It is 17% thick. At 30.8 % of the chord, the maximum thickness is reached. Figures 3.4 and Figure 3.5 represent the two sections, respectively.

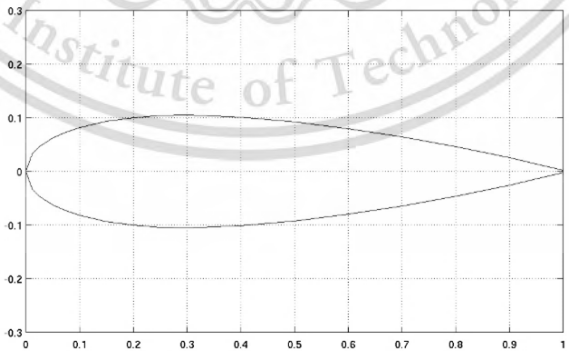

Figure 3.4 Configuration of NACA0021 airfoil

Source: UIUC Airfoil Data Site (illinois.edu)

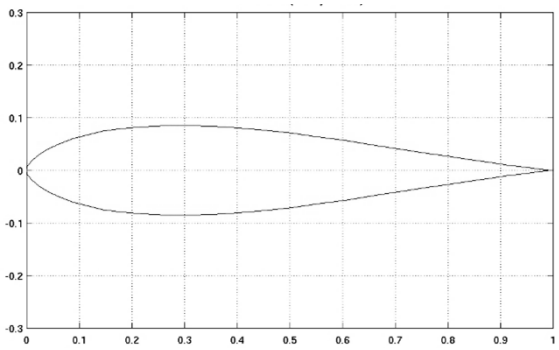

Figure 3.5 Configuration of S1046 airfoil

Source: UIUC Airfoil Data Site (illinois.edu)

The performance investigation of the turbine is examined by CFD modeling method. The parameters that affect the performance such as H/D ratio and airfoil shape are investigated.

3.2.1 Numerical Model Setup

Any fluid flow can be analyzed by using three approaches, theoretical, experimental, and numerical methods. The Navier-Stokes equations are the foundation of computational fluid dynamics (CFD), which uses numerical methods to analyze and resolve fluid flow. The principles of conservation of mass, energy, and momentum serve as the foundation for the Navier-Stokes equations, which regulate fluid dynamics [54]. In this case, the rapid speed of evaluating results is the most important aspect. In addition, CFD provides a number of benefits including being far less expensive than experimental investigations and is able to reveal the most crucial factors that might have a great deal of impact on the overall performance of turbine and the physics of the flow.

3.2.1.1. Boundary Conditions of CFD Model

The three-dimensional numerical analysis is conducted by computational fluid dynamic (CFD) using ANSYS Workbench program in order to compare the calculated numerical results and experimental results. The geometric parameters of physical model for simulation are referred to [55].

The computational domain was divided into three parts: wind tunnel region, rotor region, and blade region Boolean operations were performed to subtract the three cylindrical blade domains form the cylindrical rotor domain and to subtract the cylindrical rotor domain from the outer wind tunnel domain. An interface boundary condition was assigned at the contact surfaces of the rotating domains and the outer fixed domain. Figure 3.6 depicts the geometric model and boundary conditions and the size of each section which was determined by the rotor diameter. The data are reported in Table 3.1. The geometry of the tested model is listed in Table 3.2.

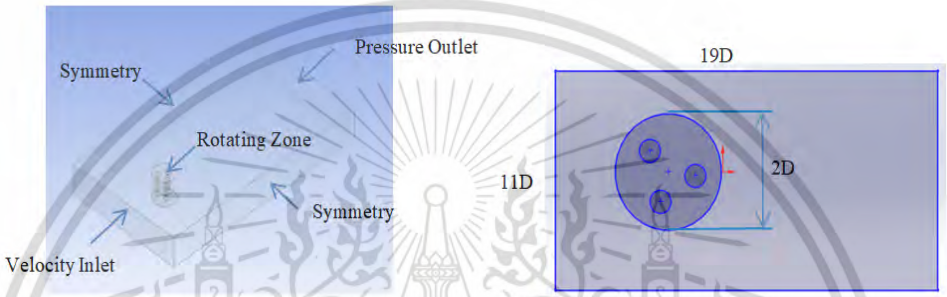

Figure 3.6 Boundary conditions and plane view of numerical model

Table 3.1 Specified dimensions of CFD domain

Domain	Denomination	Value
Wind tunnel	Length	19D
	Width	11D
	Height	2D
Rotor	Diameter	2D
	Height	1.85D
Blade	Diameter	0.5D
	Height	1.5D

Table 3.2 Geometrical features of the turbine for the validation study

Rotor Diameter	0.8m
Height of turbine	0.8m
Number of blades	3
Airfoil section	NACA 0021
Chord length	0.2m

3.2.1.2. Turbulence Model Validation

Another crucial component of the CFD technique is turbulence modeling. In various CFD models, the decision is accomplished by using turbulence models. In order to compare the numerical results of the CFD model with experimental results from the selected paper, the major objective is to establish the pattern of the turbine power coefficient as a function of tip speed ratio for all numerical investigations of this study. Two turbulence models; the Large Eddy Simulation (LES) model and the Shear Stress Transport (SST) model have been selected to predict the turbine performance.

The Large Eddy Simulation (LES) is a turbulence model that emphasizes using an adequate mesh size to resolve eddies inside the flow. It builds on the theory that the large eddies of the flow are relied on geometry while the smaller scales are more universal. This implies that large eddies can be solved implicitly, and the smaller scales can be solved through sub grid-scale model [56]. The Shear Stress Transport (SST) $k-\omega$, is a hybrid model that combines the $k-\omega$ formulation in the inner region of the boundary layer and the $k-\varepsilon$ model in the bulk flow [57]. The observations can be accurately predicted by both LES and SST models over the whole tip speed ratio range, as can be seen in Figure 3.7.

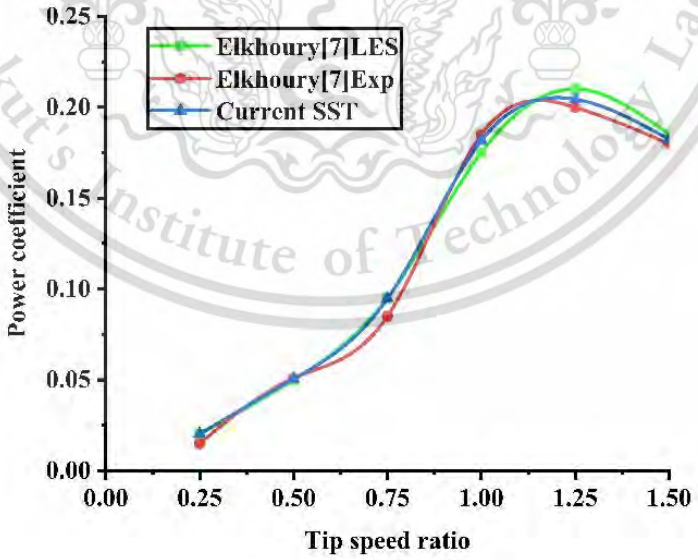

Figure 3.7 Validation of turbulence model

However, the discrepancies between the results from each model and the experimental results were measured in terms of normalized mean square error (NMSE) for the account of more accuracy. It was found that the deviation at the peak power output at the tip speed ratio of 0.25 are 0.23% and 0.048% with the LES and the SST models, respectively. Therefore, as a result of the validation study, the SST model provides a closer match to the experimental results and has been selected to evaluate the turbine performance in this study.

3.2.1.3. Mesh and Time Step Study

Mesh quality has an important influence in obtaining accurate CFD results. The capacity to predict the moment and location of flow separation around the turbine blades is the most crucial element in determining a satisfactory grid resolution. The performance of a turbine at low tip speed ratios is primarily determined by this forecast. In order to achieve faster convergence, the features of the cell size on both sides of the interface (rotor sub-grid and fixed sub-grid regions and rotor sub-grid and blades sub-domains) are the same. Numerical simulations were carried out using three different mesh sizes to make sure that the answer is independent of the mesh size. The element numbers are 2717718, 3623942 and 4044312, which define as coarse, medium, and fine respectively.

The boundary layers of 15 and the surface growth rate of 1.2 were applied to the mesh inflation to ensure a sufficient boundary layer. Mesh quality was checked in terms of skewness around the blades and the overall domain and the angle of skewness of the cells is 0.9. Mesh independence was performed with NACA0021 airfoil at wind speed of 8 m/s and tip speed ratio of 0.25. Table 3.3 shows the number of nodes, mesh elements, and the value of the average torque generated by the rotor blades for three cases.

Table 3.3 Number of studied nodes and elements

Condition	Nodes	Elements	Average torque (Nm)
Coarse	941749	2717718	1.9668
Medium	1188335	3623942	2.2035
Fine	1288912	4044312	2.1764

As simulation results indicated that for mesh element numbers 2717718 and 4044312 have a difference of less than 0.5%, the coarse mesh was set up for the fixed domain to obtain the accurate results and to save computational time. The finest unstructured mesh was used in the rotating domains with specific sizing and inflation layers to be accurate for solving near-wall flow field around the rotor blades. Figure 3.8a presents the overall picture of the final mesh where a coarse mesh was applied outside the rotor domain which has three cylindrical domains inside that cover each blade as shown in Figure 3.8b.

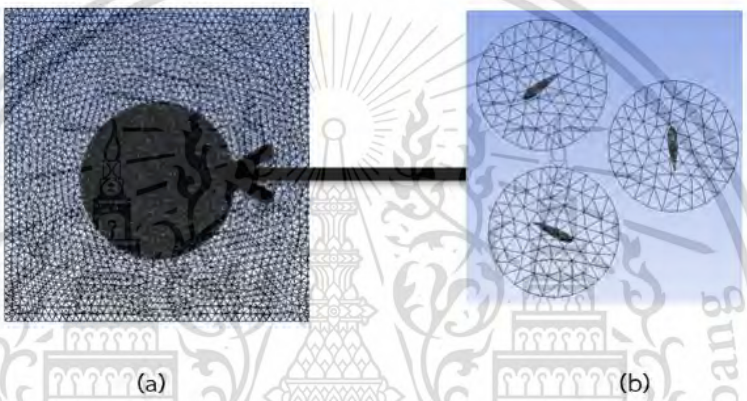

Figure 3.8 Mesh near surface clustering of the CFD domain

3.3 Wind Turbine Modeling

The power output from the chosen turbine will be incorporated into the system using the following equation.

$$P_w = 0.5\rho A V^3 C_p(\lambda, \beta) \tag{3.4}$$

where, P_w is the wind power, ρ is the air density, A is the swept area of the turbine, V is the wind speed and C_p is the power coefficient which is a function of both tip speed ratio λ and blade pitch angle β.

$$C_p(\lambda,\beta) = 0.22\,[\frac{16}{\lambda_i} - 0.4\beta - 5]e^{\frac{-12.5}{\lambda_i}} \tag{3.5}$$

where λ_i is given by

$$\frac{1}{\lambda} = \frac{1}{\lambda+0.08\beta} - \frac{0.035}{\beta^3+1} \tag{3.6}$$

The wind power generation system is modeled by MATLAB/SIMULINK as shown in Figure. 3.9. The wind speed is obtained by multiplying a random speed derived from the white noise block in SIMULINK to evaluate the wind speed fluctuation in Figure 3.9. As a result, this allows to calculate the wind power output profile utilized in this chapter. The wind speed and the wind power output profiles are presented in Figure 3.10.

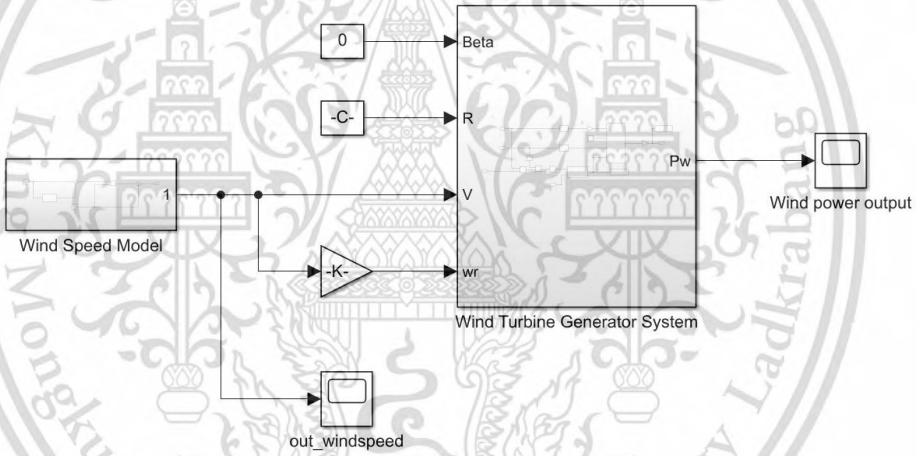

Figure 3.9 Wind Power Generation System

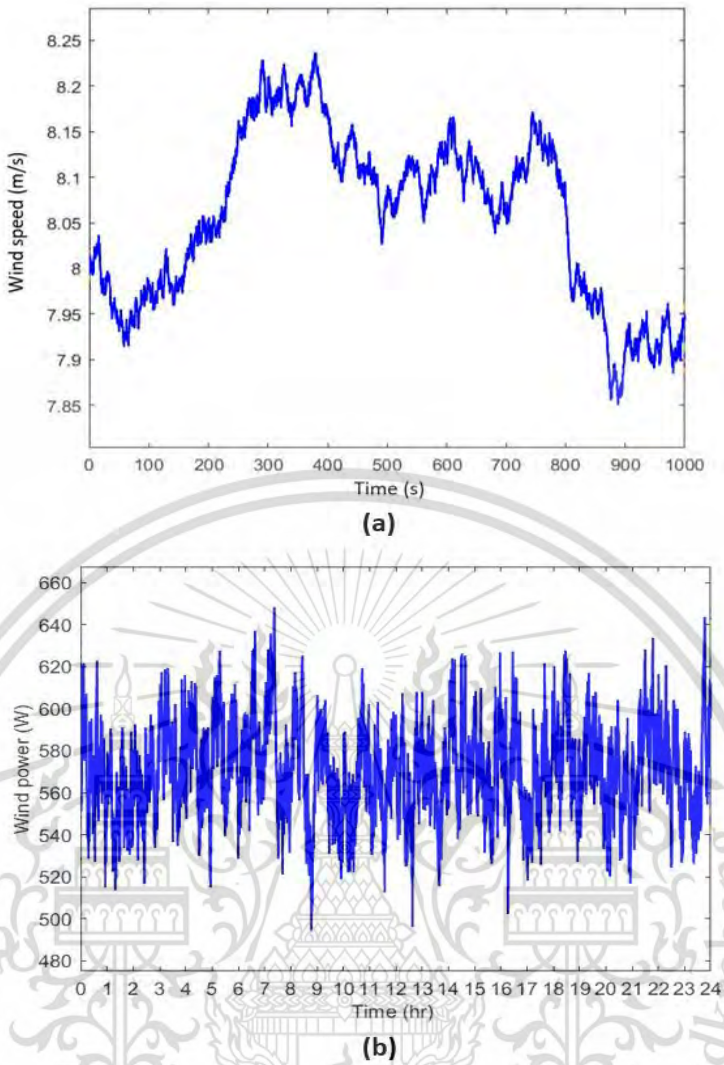

Figure 3.10 (a) Wind speed profile (b) Wind power profile

3.4 Modeling of Battery Energy Storage System

A lithium-ion battery (NCA battery) has been modeled by using MATLAB Simulink in reference to the R_{int} model presented in [58]. Table 3.4 shows the specifications of NCA battery. V_{OCV} is open circuit voltage of BESS, R_{bat}^{int} is interior resistance of BESS, and η is charge and discharge rate. V_{OCV} and R_{bat}^{int} are determined by using look-up tables based on experimental data. Figure 3.11 shows the schematic diagram of the above-mentioned battery equivalent circuit model. Figure 3.12 and Figure 3.13 present the characteristics of open circuit voltage and interior resistance via battery SOC, respectively. Generally, I_{bat} and V_{bat} can be expressed as (3.7) and

(3.8), respectively while the power consumption of battery is P W. The SOC in this study is calculated by (3.11) and the charging efficiency η is calculated based on the battery charge/discharge rate as shown in (3.12). A dynamic model of battery energy system is presented in Figure 3.14 and the discharging characteristics of employed battery is shown in Figure 3.15.

$$I_{bat} = \frac{V_{OCV} - \sqrt{V_{OCV}^2 - 4R_{bat}^{int} P}}{2R_{bat}^{int}} \tag{3.7}$$

$$V_{bat} = V_{OCV} - R_{bat}^{int} I_{bat} \tag{3.8}$$

$$V_{OCV} = f_1(SOC) \tag{3.9}$$

$$R_{bat}^{int} = \begin{cases} R_{ch} = f_2(SOC) & charging \\ R_{dis} = f_3(SOC) & discharging \end{cases} \tag{3.10}$$

$$SOC = SOC_{ini} - \int \frac{\eta I_{bat}}{Q} dt \tag{3.11}$$

$$\eta = \begin{cases} \eta_{ch} = \frac{V_{ocv}}{V_{ocv} - I_{bat} R_{ch}} & charging \\ \eta_{dis} = \frac{V_{ocv} - I_{bat} R_{dis}}{V_{ocv}} & discharging \end{cases} \tag{3.12}$$

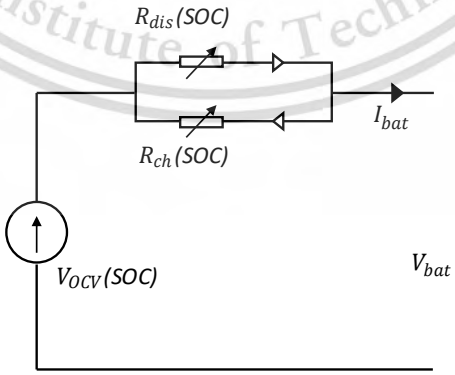

Figure 3.11 Schematic diagram of battery equivalent circuit

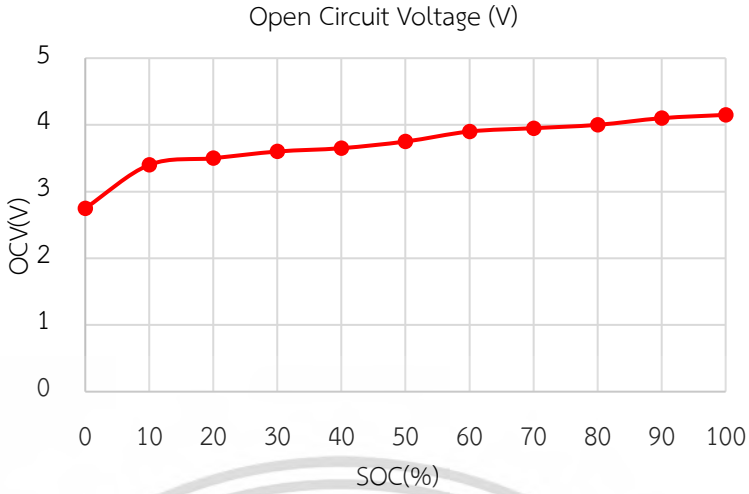

Figure 3.12 Open circuit voltage characteristic with battery SOC

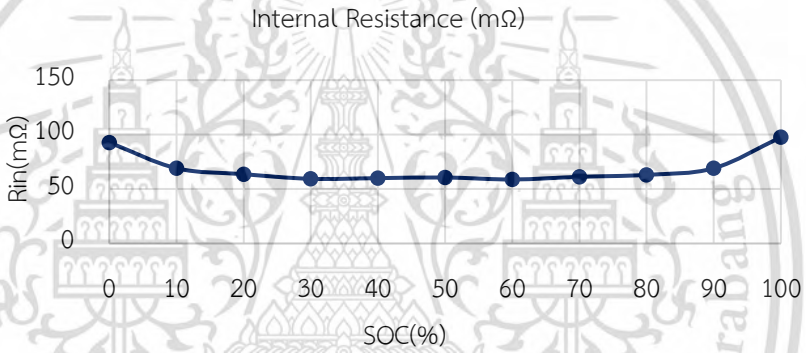

Figure 3.13 Internal resistance characteristic with battery SOC

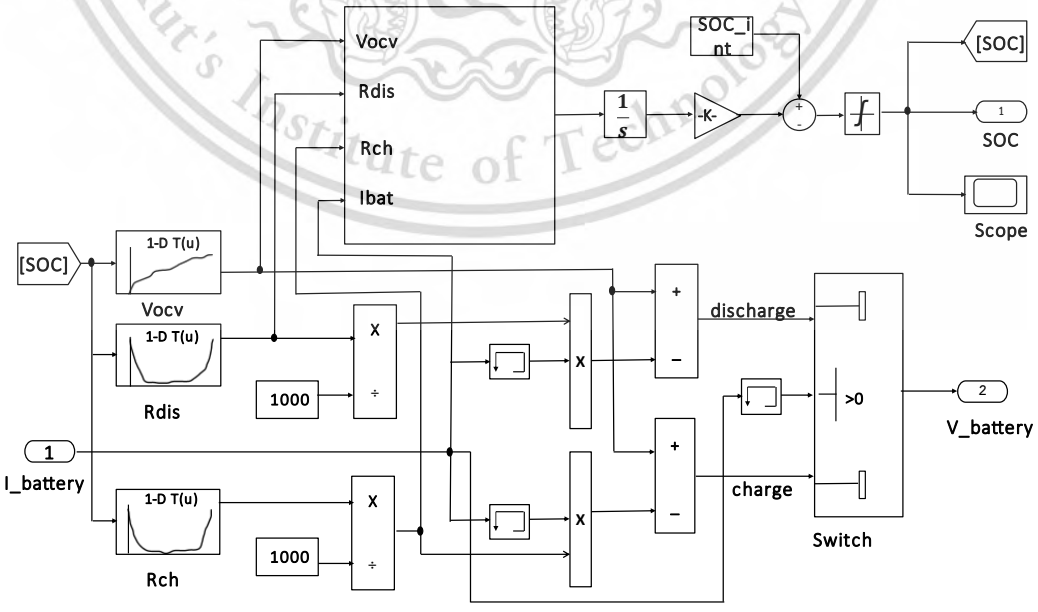

Figure 3.14 Model of Battery energy storage system

Table 3.4 Specification of Battery Cell, NCR18650GA

Rated capacity		3300mAh
Nominal voltage		3.6V
Maximum Pulse Discharge Current		3.3A
Charging voltage		4.2V
Energy density	Volumetric	693 Wh/l
	Gravimetric	224 Wh/kg
Weight(max)		48.0g

3.4.1 Capacity Configuration of Charging Station

The EV charging station being considered incorporates a wind power source and DC power chargers for charging electric vehicle (EV) batteries. The specifications and limitations established for the wind turbine and EV charging system are applicable to a particular type of EV being considered. as presented in Table 3.5.

Table 3.5 Specifications of EV bus

Item	Description
Product Type	High energy application
Vehicle Type	HEV passenger car, HEV commercial vehicle, BEV passenger car, BEV commercial vehicle, PHEV
Rated voltage	202.86 V
Rated capacity	173 Ah
Rated power	35094.78 Wh

The charging station is coupled to a dual converter, which helps to manage the power flow by switching the direction of flow at the particular time. The considered EV bus can be charged in accordance with its initial state of charge (SOC). The SOC is defined as the ratio of the available capacity to the peak capacity when the battery is fully charged. Thereupon, it indicates the remaining charging percentage of the battery. The criteria defined for the charging of EV are mathematically addressed as follows.

$$SOC_{min} \leq SOC(t) \leq SOC_{max} \tag{3.13}$$

where SOC_{min}, SOC_{max} are the minimum, the maximum SOC values respectively and $SOC(t)$ is present SOC value at the particular time. The whole charging process is considered as a constant voltage charging phase with a constant power since the electricity for EV charging primarily derives from the constant voltage stage and the fluctuations of charging power at this stage are relatively low and can be negligible. The charging duration is significantly affected by battery capacity, initial SOC, expected SOC and charging power, and is calculated as presented in (3.14).

$$T_{cev} = \frac{SOC_E - SOC_S}{\eta P} E \tag{3.14}$$

where T_{cev} is the charging duration. SOC_E is the expected SOC. SOC_S is the start SOC. P is the charging power. E is the battery capacity. η is the charging efficiency, mainly valued as 0.9.

3.4.2 Load Demand of EV

The power of EV when it arrived at charging station is calculated as;

$$P_{EV}(t) = \frac{E_{max} \cdot SOC(t)}{100\Delta t} \tag{3.15}$$

where $P_{EV}(t)$ is the power of EV at the instant time t, E_{max} is the maximum capacity of EV vehicle, and Δt is time interval considered as one hour. The load demand of EV at interval time t is evaluated as;

$$P_{DEV}(t) = \frac{E_{max} \cdot SOC_{critical}}{\Delta t} - P_{EV}(t) \tag{3.16}$$

The charging requirement of EV is determined by comparing the SOC at time t with the defined critical SOC, $SOC_{critical}$, which is considered as 0.1. In this study, the

charging station is considered to charge 5 particular EV buses. The algorithm at the charging station is shown in Figure 3.

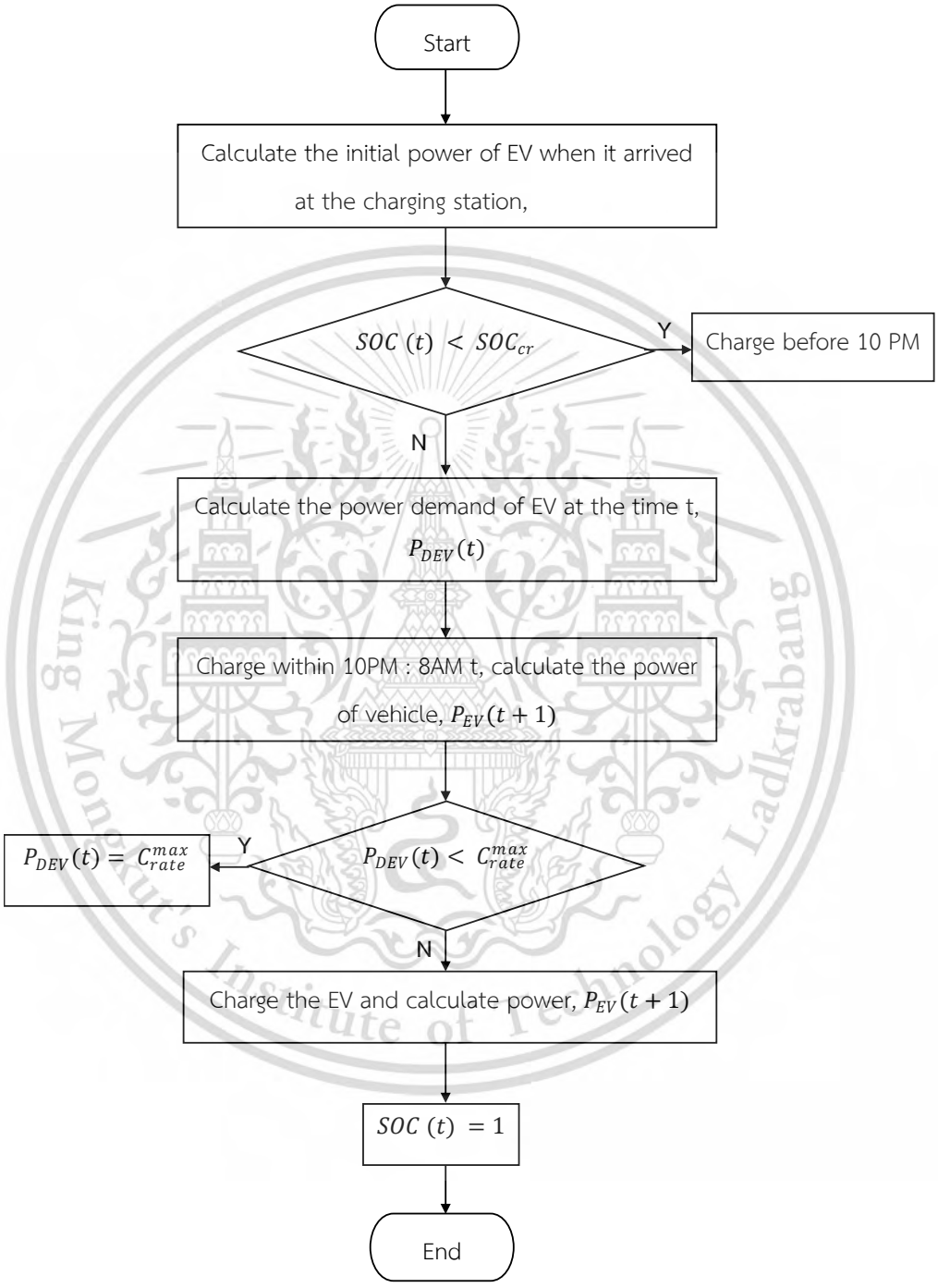

Figure 3.15 EV charging algorithm at charging station

3.5 Modeling of the Overall wind power system

The grid-connected wind-BESS power system for an EV charging station in this study consists of wind turbines, battery energy storage system, utility grid and dump load. As shown in Figure 3.16, the wind turbine, the BESS at charging station and EV load are connected to DC bus while grid and dump load are connected to DC bus via bidirectional converter.

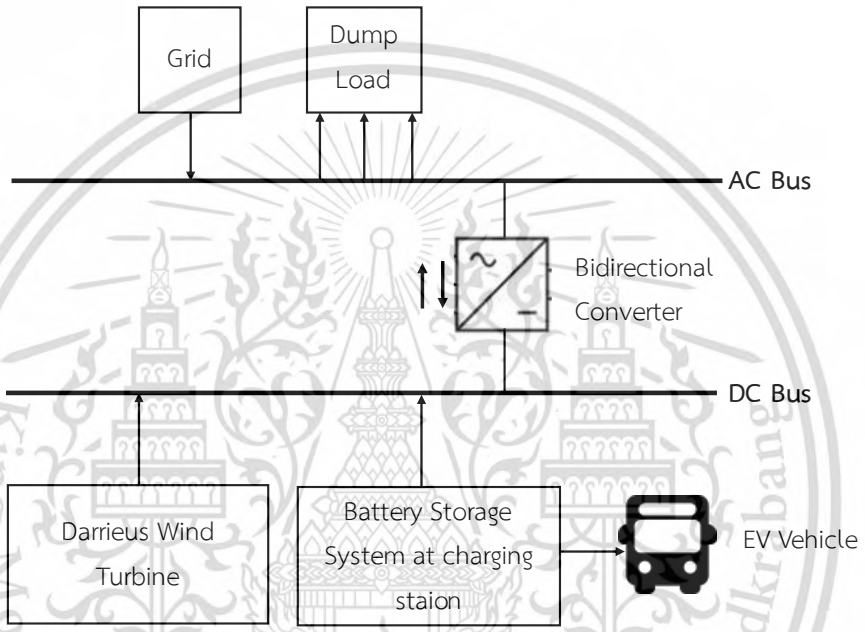

Figure 3.16 Schematic diagram of proposed power supply system

The primary source of power to charge EV buses is wind energy. In order to have less interaction with the grid, the amount of electricity purchased and sold to the grid is limited to 10 kWh maximum.

When electricity generated by wind exceeds immediate demand, a battery storage system is employed to manage the surplus energy. When the battery storage system is full and there is excess energy, it is sold to the grid if it is not over the maximum limit. If it is over the maximum limit, a dump load is activated to divert it. These dump loads can take various forms, such as air or water heaters, and are used to shunt the surplus energy produced by wind turbine system, preventing it from going to waste.

When wind energy is not enough to meet demand, the BESS provides energy to charge the EVs until it reaches the minimum SOC. Then when BESS is not enough to fulfill the demand too, the required electricity is purchased from the grid. However, the required electricity amount must not exceed the maximum limit. In the situation where both wind and BESS do not meet the demand, and the required electricity is more than the maximum purchased amount from the grid, then the system results in a loss of load supply (LPSP). An algorithm calculates the least loss of power supply probability (LPSP) while satisfying the other constraints.

3.5.1 Energy management allocation

It is considered that all the EVs arrive at the charging station at 10PM and park throughout the night until 9AM. The power management system at charging station is determined according to the available wind power and SOC of EVs when arrived at the charging station. The amount of electricity that can be purchased from and sold to the grid is limited to 10kWh. The difference between the generated power and the amount of load demand is calculated as;

$$\Delta P(t) = P_{WT}(t) - P_{DEV}(t) \tag{3.17}$$

Depending on the $\Delta P(t)$, operational strategies are determined as follows.

1) When $\Delta P(t) > 0$, the power generated from the wind turbine is sufficient enough to charge the EV and the surplus energy is stored in BESS. When there is extra power at the maximum SOC of BESS, it can be sold to the grid and is computed as;

$$P_{GS}(t) = [P_{WT}(t) - P_{DEV}(t) - P_{BESS}(t)]\,\eta_{inverter} \tag{3.18}$$

2) When $\Delta P(t) - P_{BESS}(t) > P_{GS}^{max}$, the excess power is given to the dump load, which is calculated as;

$$P_D(t) = P_{WT}(t) - P_{DEV}(t) - P_{BESS}(t) - P_{GS}^{max}/\eta_{rectifier} \tag{3.19}$$

3) When $\Delta P(t) < 0$, the wind power is not sufficient to charge EV and therefore, the amount of power required is drawn from the BESS . If both wind power and BESS are not enough for the load demand, the system is required to purchase electricity from the grid and the purchased power from the grid is calculated as;

$$P_{GP}(t) = [P_{WT}(t) + P_{BESS}(t) - P_{DEV}(t)] / \eta_{rectifier} \quad (3.20)$$

4) When $\Delta P(t) = 0$, the load demands are fulfilled by the wind power and there is no exchange power with the gird.

When the amount of power purchased from the grid is greater the limited maximum purchasing amount, $P_{GP}(t) > P_{GP}^{max}$, it defines both wind power and grid are not able to satisfy the demand. As a result of this case, a power deficiency has occurred. Power deficiency is given as;

$$P_{DEF}(t) = P_{GP}(t) - P_{GP}^{max}(t) \quad (3.21)$$

In order to ensure the load demand is satisfied reliably, the power deficiency must be equal to zero or less than zero. In this situation, the power deficiency is maintained by the constraint, LPSP. LPSP is considered 1% as the maximum limit in this study.

The simplified energy management algorithm is demonstrated with a flow chart as presented in Figure 3.17.

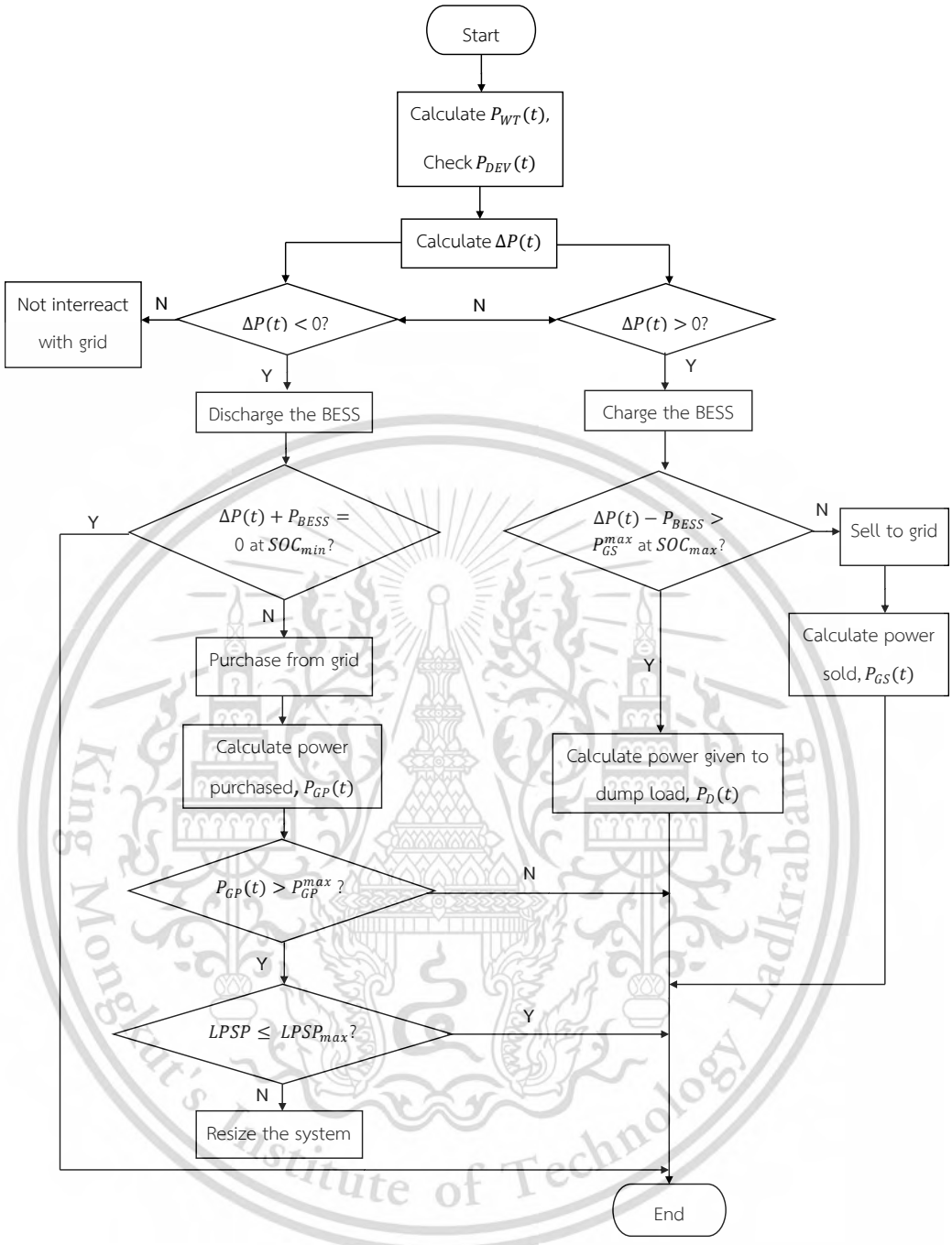

Figure 3.17 Operation strategy of proposed optimization system

3.5.2 Evaluation of reliability

Due to the fundamental intermittent nature of wind energy, analysis of feasibility plays a vital role in implementing such power supply system. A dependable electrical power system refers to a system that possesses adequate power to meet

the required load within a designated timeframe or a system that has a minimal likelihood of experiencing power supply interruptions. A reliability indicator, Loss of Power Supply Probability (LPSP) is adopted as a technical objective in this study. It is a feasibility measurement of how well the system performs under assumed or known load conditions [59].

LPSP refers to the proportion of the overall energy deficits to the total energy demand of the load during a specific chosen duration. In other words, it is the probability that a power system results in insufficient power that fails to meet the demand. LPSP is defined as ranging from 0 for the condition when load is always satisfied to 1 for the condition when load is never satisfied.

In order to make sure the total load demand is satisfied when minimizing the LPSP, which is considered to be 1% as the maximum limit to maintain within a certain tolerance range. The LPSP can be expressed as follows.

$$LPSP = \frac{\sum_{t=1}^{8760} P_{DEF}(t)}{\sum_{t=1}^{8760} P_{DEV}(t)} \tag{3.22}$$

3.5.3 Objective function and constraints

This study proposes the single objective function of optimization. The optimization problem is to minimize the levelized cost of electricity (LCOE) within the reliability boundaries. The decision factors selected for optimal cost configuration of system re the number of wind turbines, N_{WT} and number of batteries, N_B. The annualized cost of system (ACS) concept is used to design the optimization problem. The ACS consists of costs of wind turbines, C_{WT}, cost of batteries, C_B , cost of converters, C_{conv}, costs of energy purchased and sold to the grid, C_{gp}, C_{gs}. ACS is calculated as follows.

$$ACS = \sum(N_{WT}C_{WT} + N_B C_B + E_{gp}C_{gp} + C_{conv} - E_{gs}C_{gs}) \tag{3.23}$$

where E_{gp} and E_{gs} are the amount of energy purchased and sold to the grid, respectively. C_{WT}, and C_B are the total costs of wind turbines and batteries including

the annual capital cost, the annual replacement cost and maintenance cost, and are calculated as;

$$C_{WT} = C_{WT}^{cap} + C_{WT}^{rep} + C_{WT}^{mnt} \tag{3.24}$$

$$C_{B} = C_{B}^{cap} + C_{B}^{rep} + C_{B}^{mnt} \tag{3.25}$$

where C^{cap} is the annual capital cost, C^{rep} is the replacement cost and C^{mnt} is the maintenance cost. The capital recovery factor ,CRF is considered to calculate the ACS as;

$$CRF\ (i,n) = \frac{i(1+i)^n}{(1+i)^n-1} \tag{3.26}$$

where i and n are the project lifetime and the interest rate, respectively. The objective function, i.e., the economic merit of system, LCOE is calculated as;

$$LCOE = \frac{ACS}{Total\ served\ energy} \tag{3.27}$$

The objective function of optimization problem is implemented by the following constraints.

$$N_{WT}^{min} \leq N_{WT} \leq N_{WT}^{max} \tag{3.28}$$

$$N_{B}^{min} \leq N_{B} \leq N_{B}^{max} \tag{3.29}$$

$$P_{GS} \leq P_{GS}^{max} \tag{3.30}$$

$$P_{GP} \leq P_{GP}^{max} \tag{3.31}$$

where N_{WT}^{min} and N_{B}^{min} the minimum number of the wind turbine and batteries, respectively. N_{WT}^{max} and N_{B}^{max} the maximum number of the wind turbine and batteries, respectively.

3.5.4 Solution algorithm

The proposed power system involves renewable energy sources, economic and reliability objectives. Hence, this power system has several decision variables occurring a complex optimization problem. This problem requires the best compromise between the objective, LCOE and the constraint, LPSP. Therefore, the proposed wind-BESS hybrid power system is optimized by using the Artificial Bee Colony (ABC) algorithm by using MATLAB software. LCOE is minimized by using ABC optimization algorithm while LPSP is maintained within desired limits.

The Artificial Bee Colony (ABC) is a high-level problem-independent algorithm that offers a set of recommendations for searching procedures. The target is to find an ideal or nearly ideal solution in the searching area. ABC algorithm is derived by forging behavior of honeybees [60].

In the ABC algorithm, the search space is treated as a food source, and the colony of bees works to explore the search space to find the best possible solution to a given optimization problem. The ABC algorithm starts with a group of potential solutions represented by bees. Each bee assesses its solution's fitness based on an objective function. The best solutions are kept, while other bees look for new solutions. The bees share information with one another about the fitness of their solutions and promising food sources. The algorithm balances between exploring new areas and exploiting promising ones that have already been found. The implementation of ABC algorithm is presented in Figure 3.18.

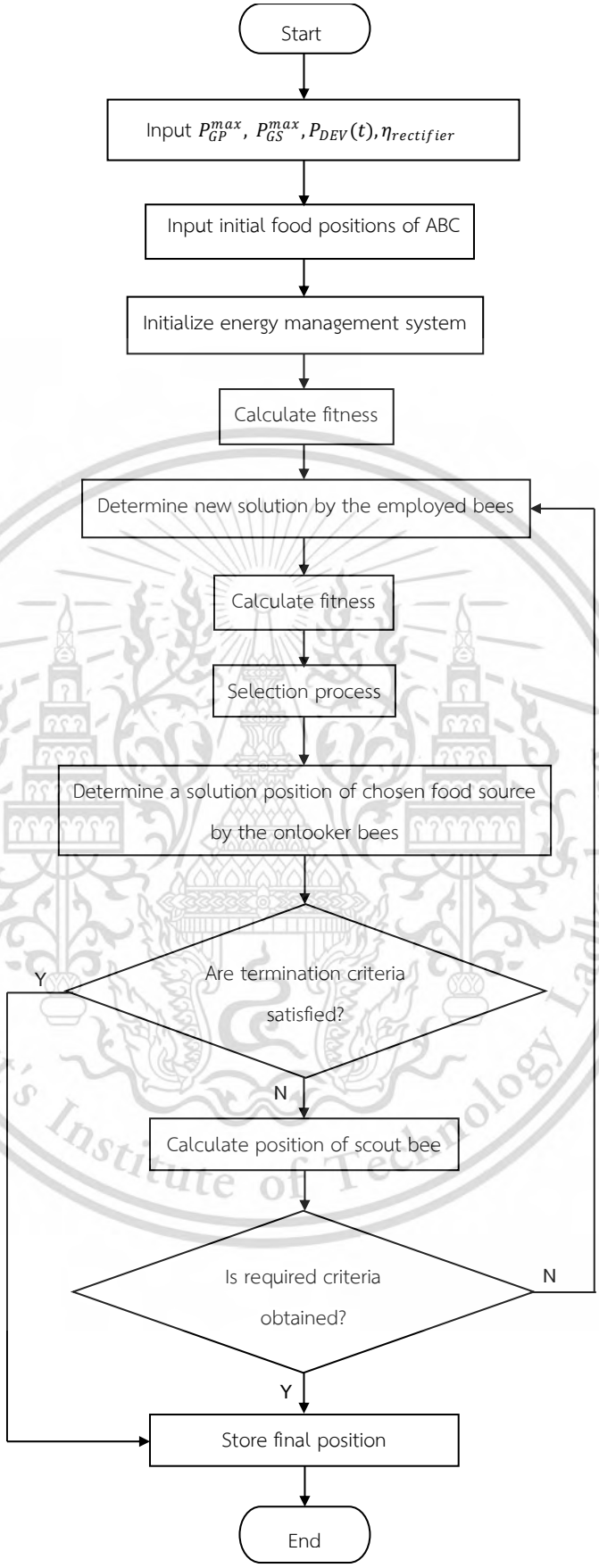

Figure 3.18 ABC algorithm flow chart

CHAPTER 4
RESULTS AND DISCUSSIONS

This chapter describes the nature of wind speed distributions, the results of wind turbine performance investigation, and the feasibility analysis of energy management system. The feasibility analysis presented regarding the use of Thai wind data includes the economy analysis and sensitivity analysis of proposed energy system.

4.1 Wind potential

An estimation of the Weibull distribution of wind frequency is presented in Figure 4.1. It was found that the wind speed at this location ranges from 2 to 9 m/s. The estimation of Weibull parameters revealed that shape and scale factors are 1.9 and 2.85, respectively.

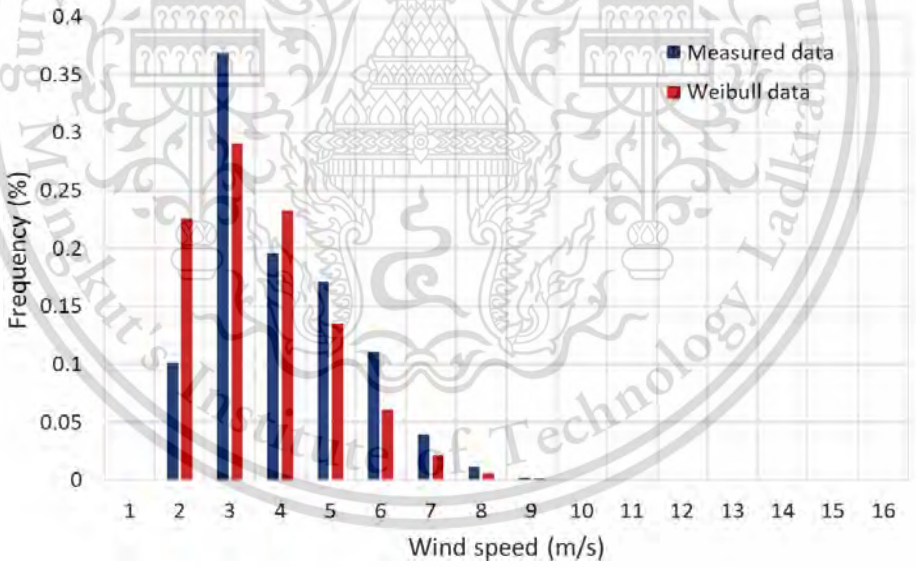

Figure 4.1 Frequency distribution of the measured wind data

The modifications of shape factor and scale factor are made to examine the impact of wind characteristics on the total energy output. As shown in Table 4.1, the scale factor form the baseline Weibull distribution is maintained constant while the shape factor is changed and vice versa. The effect of Weibull factors on wind energy

production is investigated in annual energy production (AEP) by employing the available wind data.

Table 4.1 Weibull factors of study cases

Case	Shape factor	Scale factor
Baseline	1.9	2.85
1	1.5	2.85
2	2.0	2.85
3	2.5	2.85
4	1.9	3
5	1.9	4
6	1.9	5

As can be seen in Figure 4.2 and Figure 4.3, the two factors have different effects on the AEP. The increase of shape factor causes the AEP curve to become narrower and tend toward the lower wind speed range. The value of AEP decreases with the increasing shape factor values as 604, 401, and 332 kWh, respectively. In contrast, the increase of scale factor extends the AEP curve to the higher wind speed range and dramatically increases AEP value from 700 kWh to 2,950 kWh. Accordingly, the wind measurement of the site should be considered with a high value of scale factor and a low value of shape factor since the scale factor has more significant effect on the wind distribution.

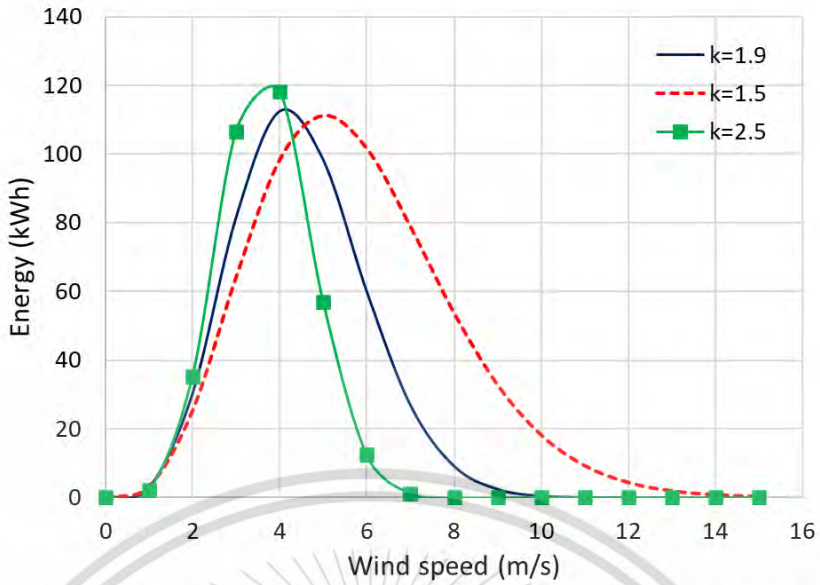

Figure 4.2 Wind AEP with different Weibull shape factor

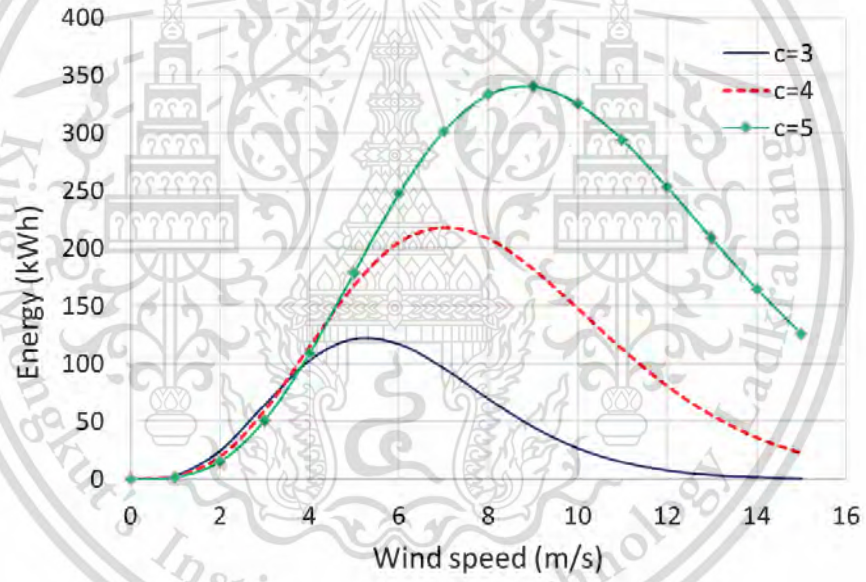

Figure 4.3 Wind AEP with different Weibull scale factor

4.2 VAWT performance investigation

The effect of solidity, airfoil profiles and rotor configuration are numerically investigated. The results are examined in terms of power coefficient.

4.2.1 Effect of solidity

The solidity effect of the VAWT is investigated for H-rotor turbine consisting of the NACA0021 airfoil and S-1046 airfoil. The solidity effect on the model with NACA0021 is similar to the model with S-1046. As power coefficient at different solidities are studied, the results showed that the power coefficient curve has been shifted lift with increasing solidity, Figure 4.4, and Figure 4.5. The higher solidity affects the air flow around the turbine and significantly reduces wind speed passing through the turbine. This is the main reason solidity affecting power performance and it reveals the wider operating is obtained at low solidity.

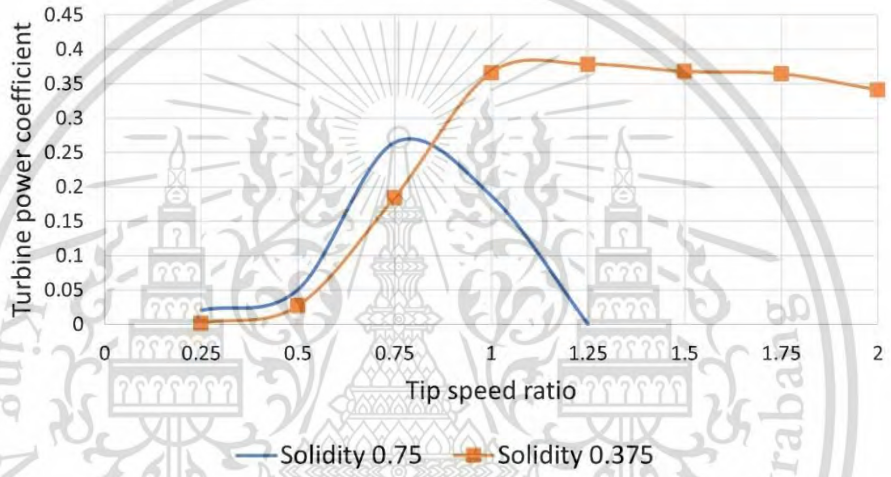

Figure 4.4 Solidity effect on the performance of H-rotor turbine constructed by NACA0021 airfoil

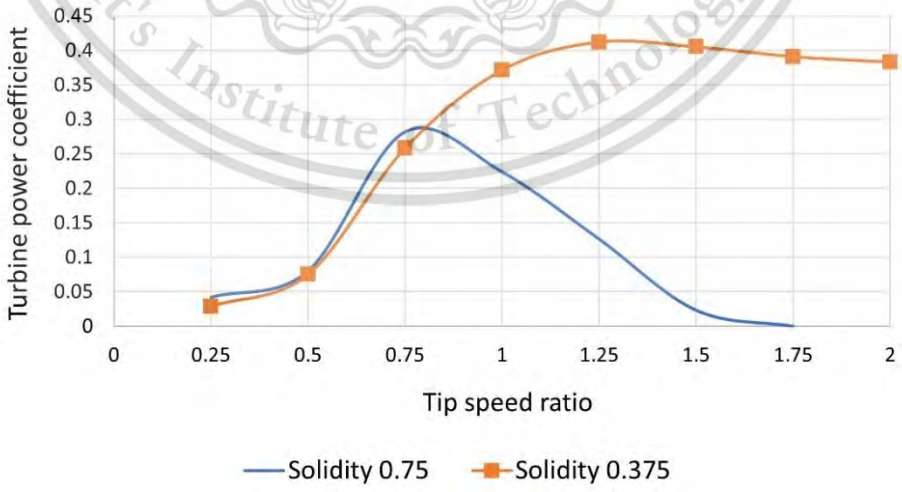

Figure 4.5 Solidity effect on the performance of H-rotor turbine constructed by S-1046 airfoil

4.2.2 Effect of rotor configuration

Three rotor configurations D01, D02 and D03 as described in Chapter 3 are investigated by modeling with two airfoils, NACA0021 and S-1046. In order to choose the most suitable rotor configuration and airfoil, the results are analyzed referring to Table 2.1 in Chapter 2.

According to the results, the rotor D01 exhibits its peak power coefficient of about 0.2 at the low tip speed ratio of 1.25 as shown in Figure 4.6 and Figure 4.7.

With the increase of the rotor diameter, rotor D02 occurs its peak power coefficient of around 0.4 at the tip speed ratio of 2. This means the increase in rotor diameter greatly affects the overall performance of the turbine. However, it can be observed that the power coefficient is very low at the low tip speed ratio range. Therefore, this turbine is not expected to have a good starting capability. It can be mentioned that the Turby wind turbine that has the H/D ratio of 1.325 is comparable to the rotor D02 in this study. The power curve of the Turby is reduced at a fast rate after the peak power in a similar manner to the D02 rotor.

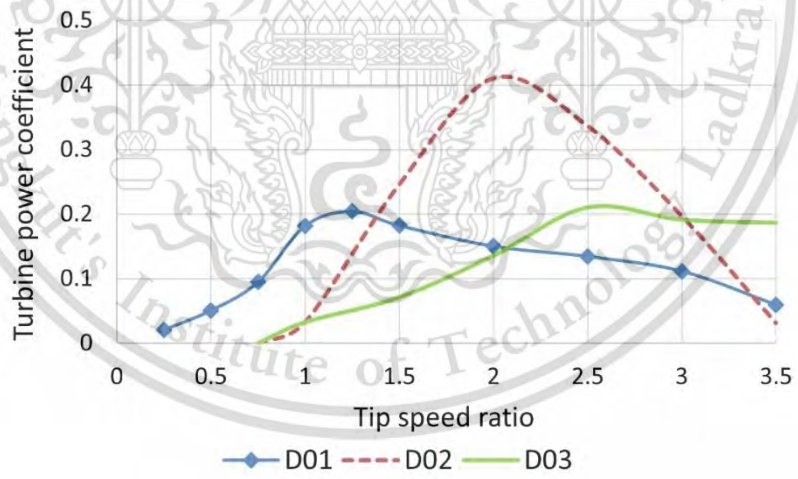

Figure 4.6 Power coefficient of different rotor configurations with NACA0021 airfoil

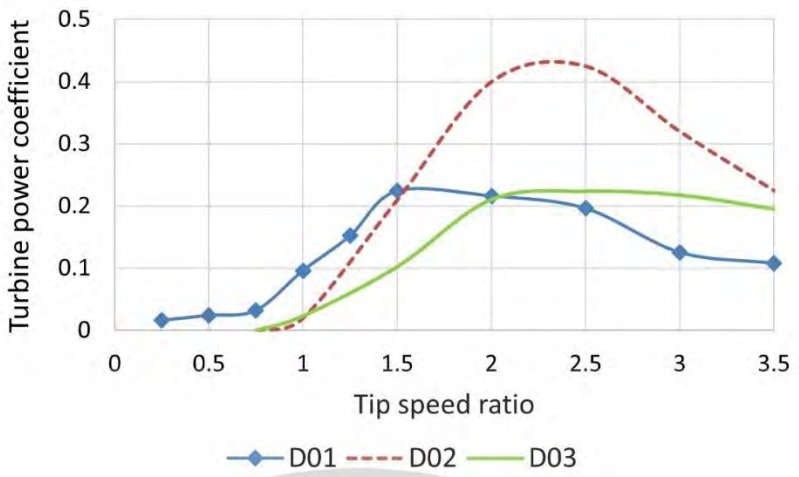

Figure 4.7 Power coefficient of different rotor configurations with S-1046 airfoil

The increase of the rotor height, rotor D03, obtains the wider operation range of turbine with a slight increase of power coefficient. As the rotor height is increased, the power curve tends to be straight and can operate with a wide range of operation such as in the case of Windspire turbine. In comparison, the power curve of Windspire turbine (Windspire) is substantially winder than the rotor D03's. This is expected to be the impact of the H/D ratio, 5.08 of Windspire. Furthermore, the Windspire turbine uses the DU-06-W200 airfoil which is projected to further improve the overall performance. The following section presents the investigation of the airfoil shape effect.

4.2.3 Effect of airfoil shape

The airfoils NACA0021 and S-1046 were employed on the three rotor configurations and the results are presented in Figure 4.8 – Figure 4.10. Despite the comparison of two airfoils in performance behavior is similar in all three turbines, the matters of tip speed ratio and operating range are significant in each case.

Figure 4.8 illustrates how the performance of D01 turbine decreased with the use of S1046 airfoil.

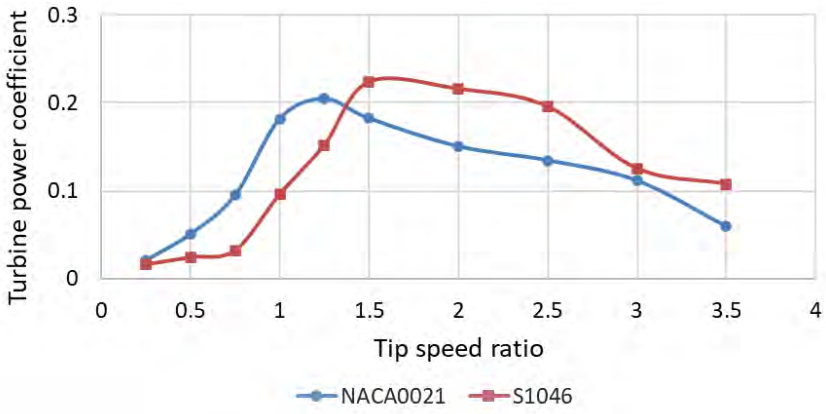

Figure 4.8 Performance of rotor D01 with two types of airfoils

The power coefficient drops at the low tip speed ratios between 0.25 and 1.25. The performance of D02 with the employment of S-1046 is still reduced at low tip speed ratios, Figure 4.9. When the tip speed ratio exceeds 2, the performance is seen to improve. According to (Mohamed M), this enhanced performance is considered to be the result of lower drag as the S-1046 was developed to have a lower drag than the NACA profiles. The leading edge of NACA airfoils is blunt and usually creates a suction peak and turbulent boundary layer on the airfoil surface.

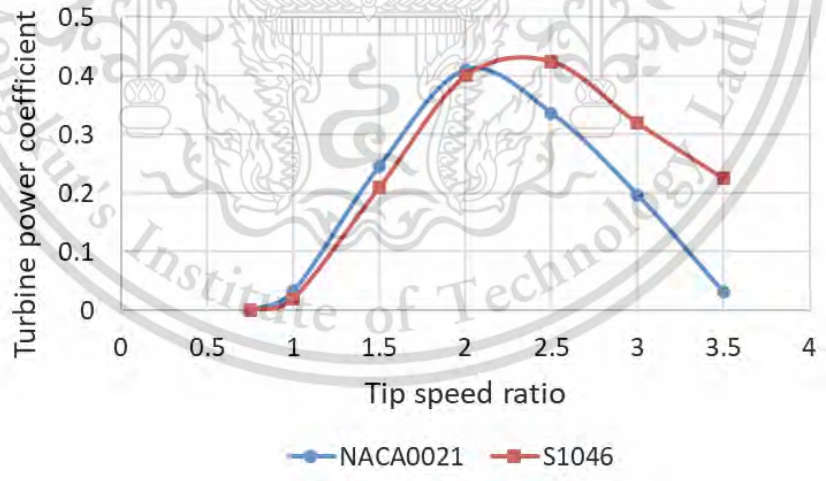

Figure 4.9 Performance of rotor D02 with two types of airfoils

As can be observed in Figure 4.10, the airfoil S-1046 outperforms the NACA0021 for the whole range of tip speed ratio except for the tip speed range lower than 1. The turbine with S-1046 airfoil occurs its maximum power coefficient at the tip speed ratio of 2.25, at which the turbine performance with NACA airfoil is slightly low. Up to the

tip speed ratio of 3.5, the employment of S-1046 makes the turbine operate with high power coefficient while that of NACA0021 seems to be decreasing.

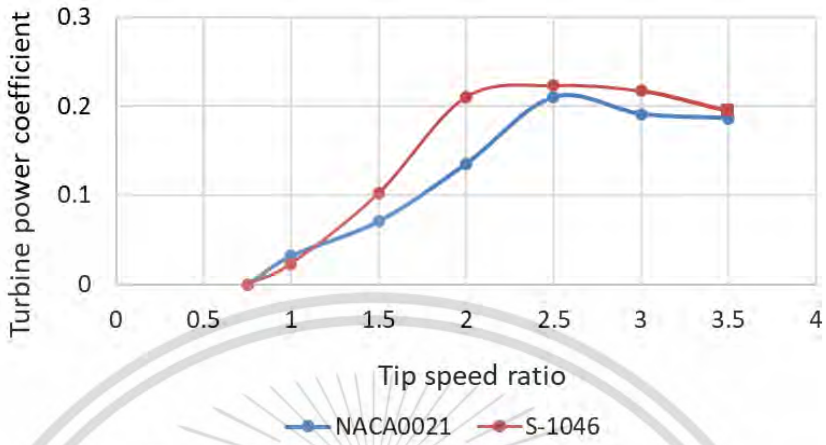

Figure 4.10 Performance of rotor D03 with two types of airfoils

It has been indicated that the rotor configuration and the airfoil shape have significant impacts on the turbine performance. Although the rotor D02 performs a considerable high-power coefficient, it will have a relatively poor starting performance as its power coefficient is very low at low tip speed ratios. In the study of rotor D03 with H/D ratio of 2, the turbine can function effectively at a variety of tip speed ratios. Nevertheless, the performance of D03 is still not much better than that of D02 for the consideration of low tip speed ratio. In all three rotor configurations, the use of S-1046 airfoil can improve the turbine performance. Nevertheless, its effectiveness is obtained by compromising with the poor performance at low tip speed ratios.

The ability to perform well at low tip speed ratio is crucial in the urban wind application because the urban wind is typically low, which operates the turbine at low tip speed ratios by spinning at a slower rotational speed. Therefore, prioritizing the performance at low tip speed ratios, the rotor D01 with the H/D ratio of 1, equipped with the NACA0021 is considered to be a promising configuration. Therefore, the Cleanfield turbine which has the H/D ration of 1.13, is then selected for the wind power generation of this study.

4.3 Wind-BESS HRE system analysis

The energy system is proposed for a lifetime of 20 years considering an interest rate of 6%. The lifetime of wind turbines, BESS and converters are considered to be the same as the system lifetime. Hence, the cost of replacement is not required. The numbers of wind turbines and batteries are optimized by the ABC algorithm. The optimization simulation is conducted by using MATLAB 2022a. The entire data of the system is considered for one year with a time interval of 1 hour.

The optimal sizings of each system components while meeting the feasibility and economic constraints are determined as the principal objective of designed optimization problem.

Table 4.2 shows the costs and specifications of the system components. The feasibility of the proposed system is investigated in terms of technical and economic reliability.

Table 4.2 Cost and specifications of system components

Component	Parameters	Value
(Vertical axis) Wind turbine	Rated power	3kW
	Rated RPM	160
	Cut-in speed	3 m/s
	Cut-out speed	45 m/s
	Number of blades	3
	Height	6 m
	Average available wind speed (at the selected location)	5.5 m/s
	Capital and replacement cost	365000 THB
	O&M cost/year	175 THB
	Life span	20 years
Battery	Rated capacity	3300 mAh
	Minimum capacity	3350 mAh
	Typical capacity	3450 mAh
	Nominal voltage	3.6 V
	Discharge end voltage	2.5 V
	Charging current (Std)	1.675 A
	Charging voltage	4.2 $\pm$ 0.03 V
	Charging time (Std)	4.0 hours
	Continuous discharge current (Max)	10 A
	Internal resistance (AC 1kHz)	$<$ 38 mΩ
	Weight	48.0 g
	Capital and replacement cost (per unit)	200 THB
	O&M cost (per unit per year)	0.29 THB
Converter	Rated power	1 kWh
	Efficiency (Rectifier & Inverter)	90 %
	Capital and replacement cost (per unit)	3800 THB
	O&M cost (per unit per year)	3.8 THB
	Life span	20 years

Figure 4.11 demonstrates the energy balance of the system at the charging station during a day. Between 9AM and 22PM, there is no EV demand at the charging station as the EVs are travelling. The amount of wind energy is enough to meet the demand most of the day. The maximum amount of available wind energy is 68.71 kWh producing the maximum surplus energy 41.63 kWh at 11AM when the EVs are not parked at the charging station. It is found that during the peak time such as between 6AM and 9AM, and after 5PM, the system is not able to have surplus energy resulting in less grid sales. During the daytime hours from 10AM to 2PM, the wind energy production is illustrated, the BESS is fully charged, and the grid sales are also at the maximum value of 10 kWh. For example, the remaining energy is 57.35 kWh, i.e., the extra energy that can be sold to the grid. Nevertheless, only the maximum capacity of grid sale 10 kWh is sold to the grid and the rest of energy 47.35 kWh goes to the dump load. It shows that the proposed energy management system is capable of providing electricity without having any unmet load. Furthermore, Table 4.3 shows the optimal sizing results of the proposed wind-BESS hybrid energy system by using ABC algorithm.

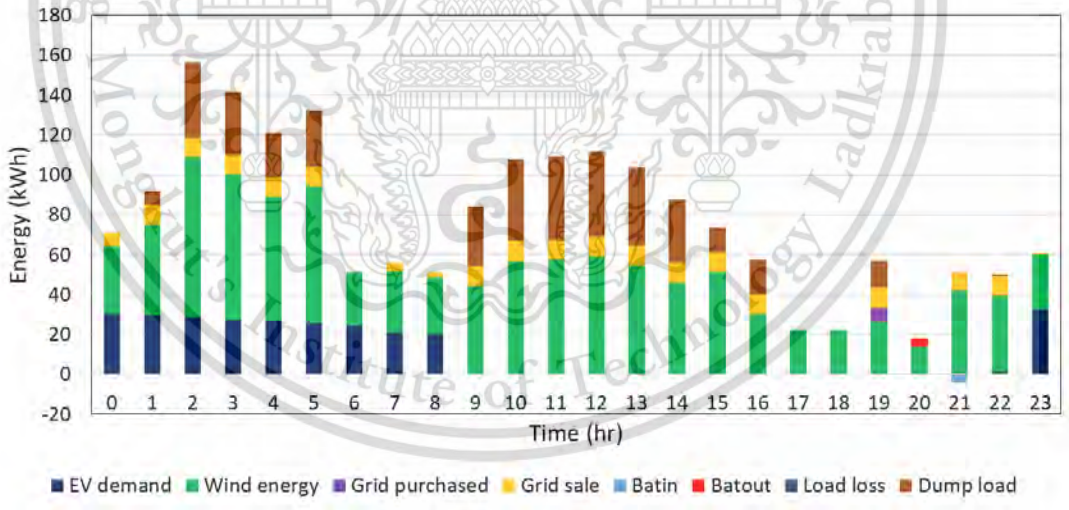

Figure 4.11 The energy balancing of the system throughout a day

Table 4.3 Optimal sizing results

Component	Wind	BESS	Converter	LCOE	NPC	ACS	LPSP
Value	3	40	1	3.5	28673001.83	2499842.96	1
Unit	kWh	kWh	kWh	THB	THB	THB	%

The annual production and consumption of each component of the system is shown in Table 4.4.

Table 4.4 Annual energy production and consumption of system

Component	Energy (kWh)
Wind	689956.16
EV demand	663291.29
Power deficiency	7417.75
Dump load	482531.41
Grid purchased	14685.24
Grid sold	56059.92
Battery charging	9628.34
Battery discharging	9657.71

4.3.1 Economic analysis

The sizings of wind turbines and BESS of the primary proposed case are 3 kW and 40 kWh, respectively. The cost division of the proposed energy system which is achieved by the ABC algorithm is presented in Table 4.5.

Table 4.5 Cost division achieved by ABC algorithm

Component	Annual cost (THB)
Wind	2559789.06
BESS	53180.73
Grid	103436.70
Inverter	5026.52
Total	2721433

Based on the optimal results, the economic assessment of the proposed system is presented. The proposed system can be profitable in the fourth year of the project lifetime as shown in Figure 4.12. The expected and actual profits are dependent on the annual outcome that consists of maintenance, operation, and replacement costs.

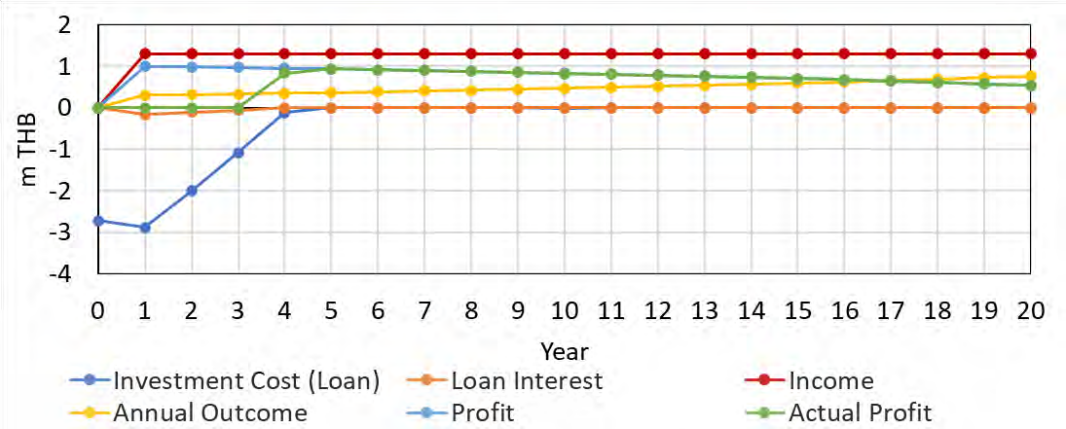

Figure 4.12 The economic assessment of the proposed system

Thereafter, the economic analysis is done by changing the sizings of the wind turbines and BESS of the proposed system to compare the value of the Net Present Cost of the system. In fact, the comparison of net present cost of system is analyzed by changing the size of rated power of wind turbine while the BESS size remains 40 kWh as presented in Figure 4.13 (a). Figure 4.13 (b) demonstrates the NPC of system when the BESS sizing is changed while the rated power of wind turbine remains at 3 kW, the same as the primary system. It can be seen that the increase of wind turbine size can dramatically vary the NPC of system. On the other hand, the change in the size of the BESS results in only a slight variation in the NPC value. That means that the rated power of wind turbines plays an important role in determining a more profitable system.

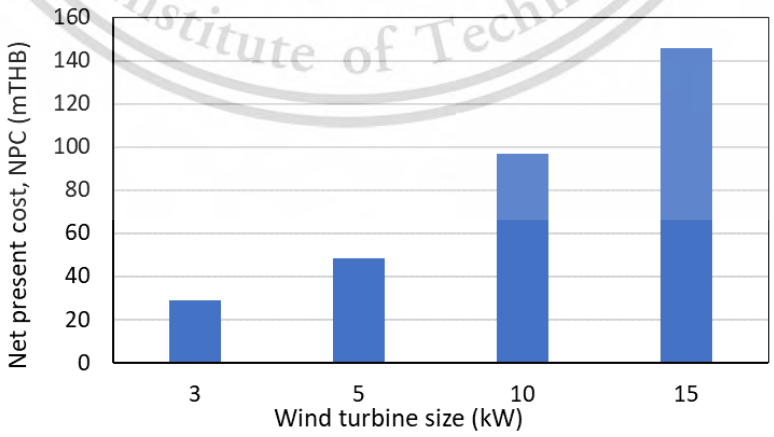

(a)

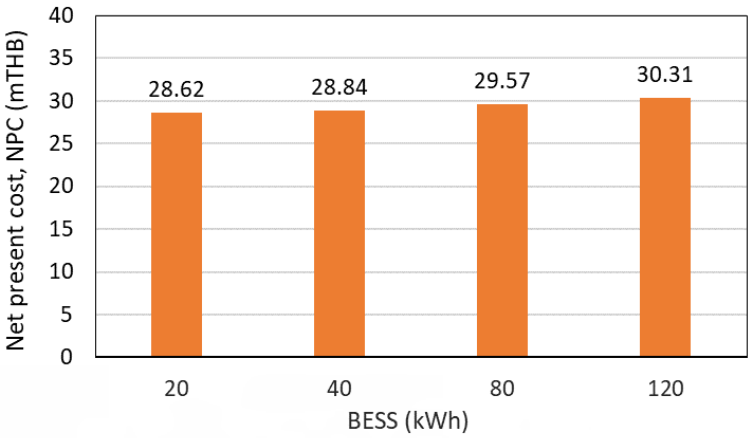

(b)

Figure 4.13 (a) Effect of wind turbine sizing on NPC value (b) Effect of BESS sizing on NPC value

4.3.2 Sensitivity analysis

The optimal system with LPSP 1% consists of 3kW wind turbines, the number of battery cells 3000 and 1kW converters. The effect of average wind speed and the capacity of maximum energy purchased and sold to the grid on the LCOE value of system are analyzed.

4.3.2.1. Effect of average wind speed

Figure 4.14 and Figure 4.15 show the effect of average wind speed on the LCOE and NPC. It can be seen that the higher average wind speed decreases the LCOE, especially once the average wind speed higher than 3m/s, 66.7% of LCOE value can be reduced. With the average wind speed range of 5-11 m/s, the LCOE is only slowly decreasing with the minimum value of 1.62 THB for 11 m/s. However, considering the NPC value, the higher wind speed may not always the feasible choices. As shown in Figure 4.15, the decrease in NPC is not very promising by applying the higher wind speed.

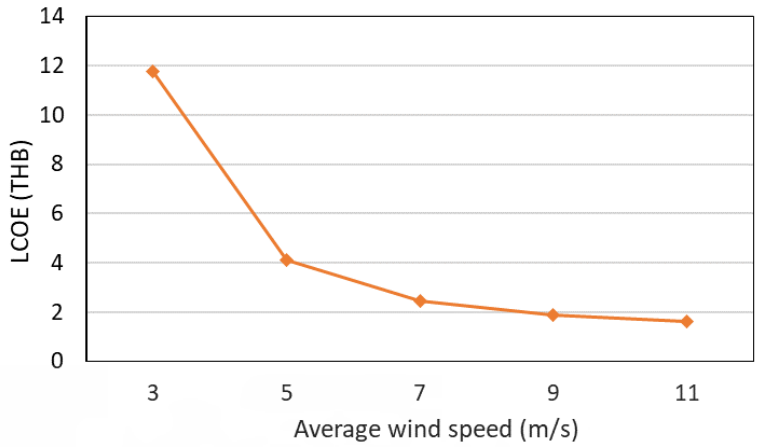

Figure 4.14 Effect of the average wind speed on the LCOE

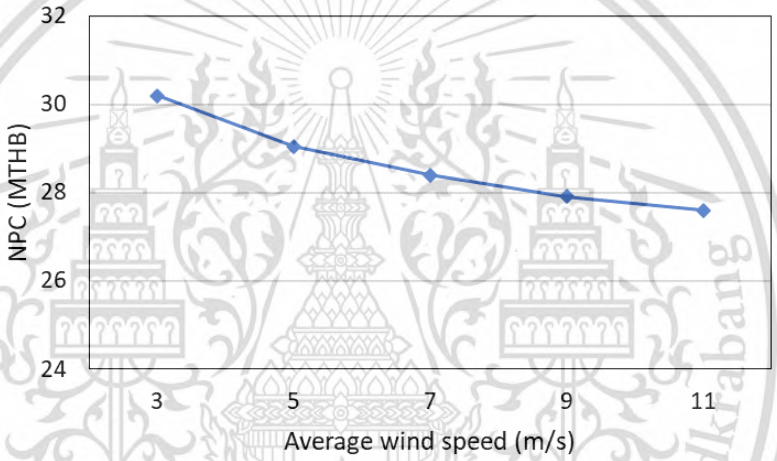

Figure 4.15 Effect of the average wind speed on the NPC

4.3.2.2. Grid capacity effect on LCOE

The capacities for power exchange with the grid, the maximum sale and purchased capacities are key parameters in a grid-connected system. The impact of grid capacities on the LCOE is investigated to examine the performance of the proposed system. Initially, the maximum grid sale is maintained at 10 kWh while the maximum grid purchased capacity is varied. Additionally, the maximum grid purchased is held at 10 kWh while the maximum grid sale capacity is varied. The changes in LCOE are evaluated. The results in Figure 4.16 can be evaluated that the increasing grid sale capacity particularly decreases the LCOE. Moreover, it can be observed that the LCOE of the system increases as the increase of maximum purchased capacity.

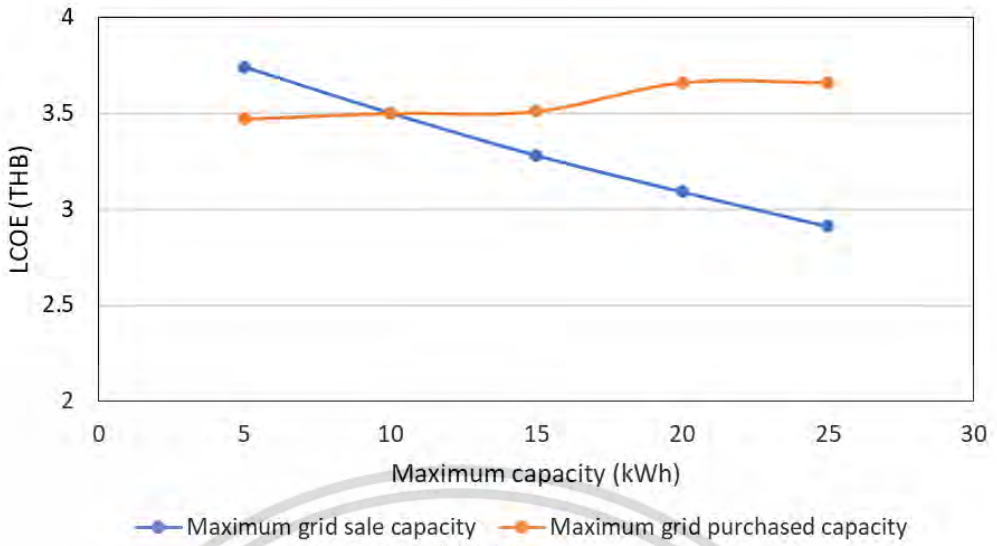

Figure 4.16 The gird capacities impact on LCOE

4.3.3 Feasibility analysis

The feasibility of wind-BESS energy system is analyzed by investigating the impact of average wind speed and BESS size on the levelized cost of electricity, LCOE. This part of the study aims to investigate the economic viability and suitability of the proposed system by evaluating the relationship between these variables.

Figure 4.17 demonstrates the relationship between the average wind speed, BESS size and the LCOE of overall system. It can be observed that as the average wind speed increases, the LCOE generally decreases for each BESS size category. This indicates that higher wind speeds contribute to more efficient power generation and lower overall cost. For an average wind speed of 3 m/s, the LCOE values are relatively higher across all BESS sizes. This suggests that at this wind speed, the system may have limited feasibility due to higher cost. As the average wind speed increases from 5 m/s to 11 m/s, the LCOE values consistently decrease. This indicates that the system becomes more economically feasible and cost-effective with higher wind speeds.

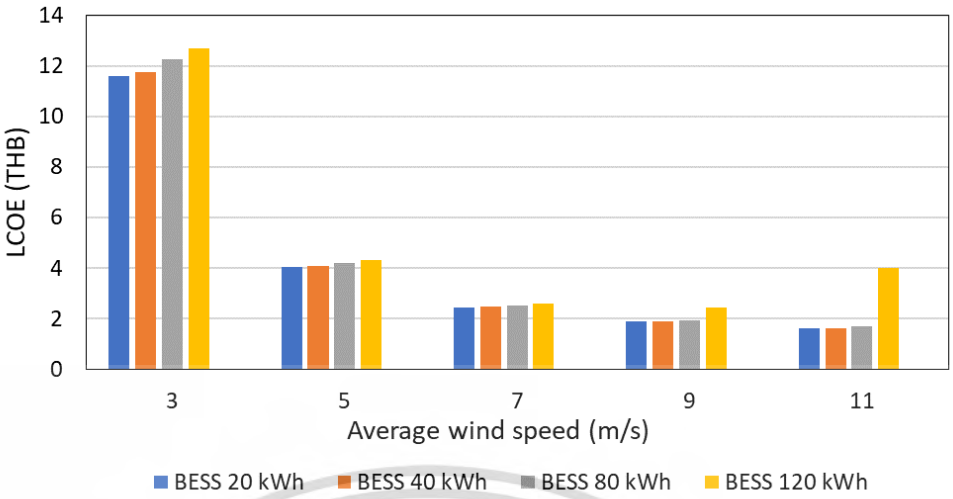

Figure 4.17 Relationship between average wind speed, BESS size and LCOE in a Wind-BESS system

Among the BESS sizes, the LCOE tends to be lower for smaller capacities (20 kWh) compared to larger capacities (120 kWh). This implies that smaller BESS sizes may be more financially feasible, potentially due to lower initial investment and maintenance costs. Increasing the BESS size generally leads to higher LCOE values, regardless of the average wind speed. This suggests that larger BESS sizes incur higher costs, potentially due to the additional investment required for larger energy storage capacities.

CHAPTER 5
CONCLUSION AND RECOMMENDATION

In the pursuit of sustainable and cost-effective energy solutions, hybrid renewable energy with battery storage systems have emerged as a promising option. These systems combine the renewable power generation capabilities of wind turbines with the energy storage capabilities of batteries to enhance grid stability and optimize energy utilization. However, assessing the feasibility of such systems requires a comprehensive analysis considering factors such as selection of wind turbine based on the wind potential of desired location, average wind speed and BESS size. The findings from the investigations of those aspects are concluded in this chapter.

5.1 Wind turbine selection for urban environments

The rotor configuration and airfoil shape have been identified as critical factors impacting turbine performance. For rotor configuration, the investigation was conducted by considering three types of rotors: square, rectangle and cylindrical configurations. The three rotors have the height to diameter ratio, H/D of 1, 0.5 and 2, respectively. For airfoil investigation, airfoil NACA001 and S1046 were utilized for equipping in the three rotors.

The rotor of H/D 0.5 demonstrates a high-power coefficient but lacks starting performance at low tip speed ratios. The rotor of H/D 2 offers a wider operational range but still falls short in terms of low tip speed ratio performance. The use of the S1046 airfoil improves overall turbine performance, however, it requires compromised performance at low tip speed ratios. Considering the significance of low tip speed ratio performance in urban wind applications, the rotor of H/D 1 and equipped with the NACA0021 airfoil emerges as the most promising choice.

Therefore, the selection of the Cleanfield V3.5 wind turbine, with an H/D ratio of 1.13, reflects the prioritization of performance at low tip speed ratios in the urban environments.

5.2 Feasibility studies of Wind-BESS energy system

In this study, a detailed mathematical model of Wind-BESS system and an operation approach for energy management are developed in order to determine the optimal sizing of the system components. The proposed system consists of 3 kW wind turbines, 40 kWh BESS, and 5.5 m/s average wind speed at considered location. Referring to Figure 4.11, Section 4.3, Chapter 4, the proposed energy system is capable of providing electricity without having any unmet load. The economic assessment based on the optimal results of the proposed system was analyzed. It can be concluded that the proposed system can start to be profitable in the fourth year of the proposed project lifetime. Therefore, the proposed model of grid-connected Wind-BESS is feasible in terms of reliability and economic factors within the required constraints.

Various investigations were analyzed in terms of economic, sensitivity and feasibility of system.

The economic investigation involved evaluating the Net Present Cost (NPC) of the system by adjusting the sizes of the wind turbines and Battery Energy Storage System (BESS). In the primary case, the wind turbine size was set at 3 kW and the BESS size at 40 kWh. By varying the rated power of the wind turbine while keeping the BESS size constant, and vice versa, the NPC of the system was compared. The results indicate that changing the wind turbine size has a significant impact on the NPC, while adjusting the BESS size only leads to minor variations. Significantly, wind turbine size of larger than 5 kW with the same availability of average wind speed can dynamically change the NPC of system. Therefore, it is evident that the rated power of the wind turbines plays a crucial role in determining the profitability of the system.

The sensitivity analysis was conducted on the average wind speed and grid capacities impact on the LCOE. The results indicated that higher average wind speeds have a significant impact on reducing the LCOE, particularly when the average wind speed exceeds 3 m/s. However, it should be noted that the decrease in LCOE becomes less significant when the average wind speed exceeds 5m/s. For the grid capacities, increasing the maximum grid sale capacity leads to a decrease in LCOE, while an increase in the maximum grid purchased capacity corresponds to an increase in LCOE.

The feasibility of wind-BESS energy system was analyzed by investigating the relationship between the average wind speed, BESS size and on the levelized cost of electricity, LCOE. The results demonstrated that higher average wind speeds generally lead to lower LCOE values, indicating improved cost-efficiency and power generation. Additionally, BESS sizes tend to result in lower LCOE values only with the suitable size for the system, suggesting that they may be more financially viable due initial investment and maintenance costs. Therefore, larger BESS sizes incur higher costs, potentially due to the increased investment required for larger energy storage capacities. The optimal combination for achieving the lowest LCOE value occurs an average wind speed of higher than 3 m/s coupled with an appropriately sized BESS smaller than 120 kWh. However, it is crucial to consider various project-specific factors and conduct a comprehensive feasibility study to accurately assess the system's viability. These factors include installation costs, operational expenses, maintenance requirements, and grid connection considerations. By taking these factors into account, a more informed decision can be made regarding the feasibility and economic viability of implementing a wind-BESS energy system.

5.3 Recommendations

The author would like to make recommendations for the current study as follows:

1. In this study, the proposed energy system consists of wind turbines, BESS, and utility grid. The load demands are only considered as DC loads. The demand for AC loads should be considered as well in order to be more reliable for urban use.
2. Further investigation about EV demand and wind availability based on Meteorological should be conducted.
3. The optimization of the system is evaluated by using only one algorithm. A comparative study by using at least one more algorithm may help to determine a more accurate and efficient solution.

BIBLIOGRAPHY

[1] M. Höök and X. Tang, "Depletion of fossil fuels and anthropogenic climate change-A review," *Energy Policy*, vol. 52, pp. 797–809, Jan. 2013, doi: 10.1016/j.enpol.2012.10.046.

[2] M. Brenna, F. Foiadelli, C. Leone, and M. Longo, "Electric Vehicles Charging Technology Review and Optimal Size Estimation," *Journal of Electrical Engineering and Technology*, vol. 15, no. 6, pp. 2539–2552, Nov. 2020, doi: 10.1007/s42835-020-00547-x.

[3] M. H. Mohamed, "Performance investigation of H-rotor Darrieus turbine with new airfoil shapes," *Energy*, vol. 47, no. 1, pp. 522–530, 2012, doi: 10.1016/j.energy.2012.08.044.

[4] I. Hashem and M. H. Mohamed, "Aerodynamic performance enhancements of H-rotor Darrieus wind turbine," *Energy*, vol. 142, pp. 531–545, Jan. 2018, doi: 10.1016/j.energy.2017.10.036.

[5] G. van Bussel, H. Polinder, and H. Sidler, "The development of Turby, a small vawt for the built environment." AWEA, pp. 1-10`, 2004. Accessed: May 29, 2023. [Online]. Available: https://research.tudelft.nl/en/publications/the-development-of-turby-a-small-vawt-for-the-built-environment

[6] V. Bostan, M. Gutu, and I. Rabei, "Development and validation of a CFD model used for vertical axis wind turbines simulations," in *IOP Conference Series: Materials Science and Engineering*, Institute of Physics Publishing, Nov. 2018. doi: 10.1088/1757-899X/444/2/022002.

[7] A. Huskey, A. Bowen, and D. Jager, "Wind Turbine Generator System Power Performance Test Report for the Mariah Windspire 1-kW Wind Turbine," 2009.

[8] K. Rogowski, M. O. L. Hansen, and G. Bangga, "Performance analysis of a h-darrieuswind turbine for a series of 4-digit NACA airfoils," *Energies (Basel)*, vol. 13, no. 12, Jun. 2020, doi: 10.3390/en13123196.

[9] R. A. Ghazalla, M. H. Mohamed, and A. A. Hafiz, "Synergistic analysis of a Darrieus wind turbine using computational fluid dynamics," *Energy*, vol. 189, Dec. 2019, doi: 10.1016/j.energy.2019.116214.

[10] F. Feng, S. Zhao, C. Qu, Y. Bai, Y. Zhang, and Y. Li, "Research on Aerodynamic Characteristics of Straight-Bladed Vertical Axis Wind Turbine with S Series Airfoils," *International Journal of Rotating Machinery*, vol. 2018, 2018, doi: 10.1155/2018/8350243.

[11] P. Sabaeifard, H. Razzaghi, and A. Forouzandeh, "Determination of Vertical Axis Wind Turbines Optimal Configuration through CFD Simulations," 2012.

[12] T. Mon and S. Worasinchai, "Effects of the-Rotor -C-onfiguration and the -Airfoil Shape on the Darrieus Wind Turbine Performance," *2021 13th International Conference on Information Technology and Electrical Engineering, ICITEE 2021*, pp. 110–115, 2021, doi: 10.1109/ICITEE53064.2021.9611958.

[13] S. Li and Y. Li, "Numerical study on the performance effect of solidity on the straight-bladed vertical axis wind turbine," in *Asia-Pacific Power and Energy Engineering Conference, APPEEC*, 2010. doi: 10.1109/APPEEC.2010.5449269.

[14] C. Liang, D. Xi, S. Zhang, and Q. Yang, "Effects of Solidity on Aerodynamic Performance of H-Type Vertical Axis Wind Turbine," in *IOP Conference Series: Earth and Environmental Science*, Institute of Physics Publishing, Jul. 2018. doi: 10.1088/1755-1315/170/4/042061.

[15] H. Kim and B. Kim, "Wind resource assessment and comparative economic analysis using AMOS data on a 30MW wind farm at Yulchon district in Korea," *Renew Energy*, vol. 85, pp. 96–103, Jan. 2016, doi: 10.1016/j.renene.2015.06.039.

[16] M. Elamouri and F. Ben Amar, "Wind energy potential in Tunisia," *Renew Energy*, vol. 33, no. 4, pp. 758–768, Apr. 2008, doi: 10.1016/j.renene.2007.04.005.

[17] E. K. Akpinar and S. Akpinar, "Statistical analysis of wind energy potential on the basis of the Weibull and Rayleigh distributions for Agin-Elazig, Turkey," *Proceedings of the Institution of Mechanical Engineers, Part A: Journal of Power and Energy*, vol. 218, no. 8, pp. 557–565, 2004, doi: 10.1243/0957650042584357.

[18] J. A. Carta, P. Ramírez, and S. Velázquez, "A review of wind speed probability distributions used in wind energy analysis. Case studies in the Canary Islands," *Renewable and Sustainable Energy Reviews*, vol. 13, no. 5, pp. 933–955, Jun. 2009, doi: 10.1016/j.rser.2008.05.005.

[19] D. M. Deaves and I. G. Lines, “On the fitting of low mean windspeed data to the Weibull distribution,” *Journal of Wind Engineering and Industrial Aerodynamics*, vol. 66, no. 3, pp. 169–178, Mar. 1997, doi: 10.1016/S0167-6105(97)00013-5.

[20] F. Noman, A. A. Alkahtani, V. Agelidis, K. S. Tiong, G. Alkawsi, and J. Ekanayake, “Wind-energy-powered electric vehicle charging stations: Resource availability data analysis,” *Applied Sciences (Switzerland)*, vol. 10, no. 16, Aug. 2020, doi: 10.3390/app10165654.

[21] J. A. Domínguez-Navarro, R. Dufo-López, J. M. Yusta-Loyo, J. S. Artal-Sevil, and J. L. Bernal-Agustín, “Design of an electric vehicle fast-charging station with integration of renewable energy and storage systems,” *International Journal of Electrical Power and Energy Systems*, vol. 105, pp. 46–58, Feb. 2019, doi: 10.1016/j.ijepes.2018.08.001.

[22] P. Goli and W. Shireen, “Wind powered smart charging facility for PHEVs,” in *2014 IEEE Energy Conversion Congress and Exposition, ECCE 2014*, Institute of Electrical and Electronics Engineers Inc., Nov. 2014, pp. 1986–1991. doi: 10.1109/ECCE.2014.6953663.

[23] H. Lund and W. Kempton, “Integration of renewable energy into the transport and electricity sectors through V2G,” *Energy Policy*, vol. 36, no. 9, pp. 3578–3587, Sep. 2008, doi: 10.1016/j.enpol.2008.06.007.

[24] H. J. Vermaak and K. Kusakana, “Design of a photovoltaic-wind charging station for small electric Tuk-tuk in D.R.Congo,” *Renew Energy*, vol. 67, pp. 40–45, 2014, doi: 10.1016/j.renene.2013.11.019.

[25] H. Fathabadi, “Novel wind powered electric vehicle charging station with vehicle-to-grid (V2G) connection capability,” *Energy Convers Manag*, vol. 136, pp. 229–239, 2017, doi: 10.1016/j.enconman.2016.12.045.

[26] T. Yi, C. Zhang, T. Lin, and J. Liu, “Research on the spatial-temporal distribution of electric vehicle charging load demand: A case study in China,” *J Clean Prod*, vol. 242, Jan. 2020, doi: 10.1016/j.jclepro.2019.118457.

[27] M. Chang, S. Bae, G. G. Yoon, S. H. Park, and Y. Choy, “Impact of Electric Vehicle Charging Demand on a Jeju Island Radial Distribution Network,” *2019 IEEE Power and Energy Society Innovative Smart Grid Technologies Conference, ISGT 2019*, Feb. 2019, doi: 10.1109/ISGT.2019.8791604.

[28] V. Prajapati *et al.*, "A literature review of state of-charge estimation techniques applicable to lithium poly-carbon monoflouride (LI/CFx) battery," in *India International Conference on Power Electronics, IICPE 2010*, 2011. doi: 10.1109/IICPE.2011.5728101.

[29] N. Watrin, B. Blunier, and A. Miraoui, "Review of adaptive systems for lithium batteries state-of-charge and state-of-health estimation," in *2012 IEEE Transportation Electrification Conference and Expo, ITEC 2012*, 2012. doi: 10.1109/ITEC.2012.6243437.

[30] C. Zhang, K. Li, S. McLoone, and Z. Yang, "Battery modelling methods for electric vehicles - A review," in *2014 European Control Conference, ECC 2014*, Institute of Electrical and Electronics Engineers Inc., Jul. 2014, pp. 2673–2678. doi: 10.1109/ECC.2014.6862541.

[31] F. Elmahdi, L. Ismail, and M. Noureddine, "Fitting the OCV-SOC relationship of a battery lithium-ion using genetic algorithm method," in *E3S Web of Conferences*, EDP Sciences, Feb. 2021. doi: 10.1051/e3sconf/202123400097.

[32] A. Hasan, M. Skriver, and T. A. Johansen, "Exogenous Kalman Filter for State-of-Charge Estimation in Lithium-Ion Batteries," *2018 IEEE Conference on Control Technology and Applications, CCTA 2018*, pp. 1403–1408, Oct. 2018, doi: 10.1109/CCTA.2018.8511577.

[33] H. G. Schweiger *et al.*, "Comparison of several methods for determining the internal resistance of lithium ion cells," *Sensors*, vol. 10, no. 6, pp. 5604–5625, Jun. 2010, doi: 10.3390/s100605604.

[34] N. Ghorbani, A. Kasaeian, A. Toopshekan, L. Bahrami, and A. Maghami, "Optimizing a hybrid wind-PV-battery system using GA-PSO and MOPSO for reducing cost and increasing reliability," *Energy*, vol. 154, pp. 581–591, Jul. 2018, doi: 10.1016/j.energy.2017.12.057.

[35] R. Dufo-López, J. L. Bernal-Agustín, and F. Mendoza, "Design and economical analysis of hybrid PV–wind systems connected to the grid for the intermittent production of hydrogen," *Energy Policy*, vol. 37, no. 8, pp. 3082–3095, Aug. 2009, doi: 10.1016/J.ENPOL.2009.03.059.

[36] G. Merei, C. Berger, and D. U. Sauer, “Optimization of an off-grid hybrid PV-Wind-Diesel system with different battery technologies using genetic algorithm,” *Solar Energy*, vol. 97, pp. 460–473, Nov. 2013, doi: 10.1016/j.solener.2013.08.016.

[37] M. H. Amrollahi and S. M. T. Bathaee, “Techno-economic optimization of hybrid photovoltaic/wind generation together with energy storage system in a stand-alone micro-grid subjected to demand response,” *Appl Energy*, vol. 202, pp. 66–77, 2017, doi: 10.1016/j.apenergy.2017.05.116.

[38] M. S. Javed, A. Song, and T. Ma, “Techno-economic assessment of a stand-alone hybrid solar-wind-battery system for a remote island using genetic algorithm,” *Energy*, vol. 176, pp. 704–717, Jun. 2019, doi: 10.1016/j.energy.2019.03.131.

[39] L. G. Acuña, R. V. Padilla, and A. S. Mercado, “Measuring reliability of hybrid photovoltaic-wind energy systems: A new indicator,” *Renew Energy*, vol. 106, pp. 68–77, 2017, doi: 10.1016/j.renene.2016.12.089.

[40] O. Ekren and B. Y. Ekren, “Size optimization of a PV/wind hybrid energy conversion system with battery storage using simulated annealing,” *Appl Energy*, vol. 87, no. 2, pp. 592–598, 2010, doi: 10.1016/j.apenergy.2009.05.022.

[41] F. Xu, J. Liu, S. Lin, Q. Dai, and C. Li, “A multi-objective optimization model of hybrid energy storage system for non-grid-connected wind power: A case study in China,” *Energy*, vol. 163, pp. 585–603, Nov. 2018, doi: 10.1016/j.energy.2018.08.152.

[42] M. A. M. Ramli, H. R. E. H. Bouchekara, and A. S. Alghamdi, “Optimal sizing of PV/wind/diesel hybrid microgrid system using multi-objective self-adaptive differential evolution algorithm,” *Renew Energy*, vol. 121, pp. 400–411, Jun. 2018, doi: 10.1016/j.renene.2018.01.058.

[43] E. L. V. Eriksson and E. M. A. Gray, “Optimization of renewable hybrid energy systems – A multi-objective approach,” *Renew Energy*, vol. 133, pp. 971–999, Apr. 2019, doi: 10.1016/j.renene.2018.10.053.

[44] A. A. Moghaddam, A. Seifi, and T. Niknam, “Multi-operation management of a typical micro-grids using Particle Swarm Optimization: A comparative study,” *Renewable and Sustainable Energy Reviews*, vol. 16, no. 2. Elsevier Ltd, pp. 1268–1281, 2012. doi: 10.1016/j.rser.2011.10.002.

[45] X. Xu, W. Hu, D. Cao, Q. Huang, C. Chen, and Z. Chen, "Optimized sizing of a standalone PV-wind-hydropower station with pumped-storage installation hybrid energy system," *Renew Energy*, vol. 147, pp. 1418–1431, Mar. 2020, doi: 10.1016/j.renene.2019.09.099.

[46] S. Singh, P. Chauhan, and N. J. Singh, "Capacity optimization of grid connected solar/fuel cell energy system using hybrid ABC-PSO algorithm," *Int J Hydrogen Energy*, vol. 45, no. 16, pp. 10070–10088, Mar. 2020, doi: 10.1016/j.ijhydene.2020.02.018.

[47] R. Das *et al.*, "Multi-objective techno-economic-environmental optimisation of electric vehicle for energy services," *Appl Energy*, vol. 257, Jan. 2020, doi: 10.1016/j.apenergy.2019.113965.

[48] A. Sagharichi, M. J. Maghrebi, and A. Arabgolarcheh, "Variable pitch blades: An approach for improving performance of Darrieus wind turbine," *Journal of Renewable and Sustainable Energy*, vol. 8, no. 5, Sep. 2016, doi: 10.1063/1.4964310.

[49] M. Islam, A. Fartaj, R. Carriveau, A. Medina, and A. Munawara, "Analysis of the Design Parameters related to a Fixed-pitch Straight-Bladed Vertical Axis Wind Turbine," 2008.

[50] N. Guillaud, G. Balarac, E. Goncalvès, and J. Zanette, "Large Eddy Simulations on Vertical Axis Hydrokinetic Turbines - Power coefficient analysis for various solidities," *Renew Energy*, vol. 147, pp. 473–486, Mar. 2020, doi: 10.1016/j.renene.2019.08.039.

[51] K. McLaren, S. Tullis, and S. Ziada, "Computational fluid dynamics simulation of the aerodynamics of a high solidity, small-scale vertical axis wind turbine," *Wind Energy*, vol. 15, no. 3, pp. 349–361, 2012, doi: 10.1002/we.472.

[52] K. Rogowski, M. O. L. Hansen, and G. Bangga, "Performance analysis of a h-darrieuswind turbine for a series of 4-digit NACA airfoils," *Energies (Basel)*, vol. 13, no. 12, Jun. 2020, doi: 10.3390/en13123196.

[53] M. A. Singh, A. Biswas, and R. D. Misra, "Investigation of self-starting and high rotor solidity on the performance of a three S1210 blade H-type Darrieus rotor," *Renew Energy*, vol. 76, pp. 381–387, Apr. 2015, doi: 10.1016/j.renene.2014.11.027.

[54] K. M. Almohammadi, “Optimization of a CFD based design of a straight blade vertical axis wind turbine (SB-VAWT),” 2014, Accessed: May 29, 2023. [Online]. Available: https://etheses.whiterose.ac.uk/7021/

[55] M. Elkhoury, T. Kiwata, and E. Aoun, “Experimental and numerical investigation of a three-dimensional vertical-axis wind turbine with variable-pitch,” *Journal of Wind Engineering and Industrial Aerodynamics*, vol. 139, pp. 111–123, Apr. 2015, doi: 10.1016/J.JWEIA.2015.01.004.

[56] H. Schlichting and K. Gersten, “Boundary-Layer Theory,” *Boundary-Layer Theory*, pp. 1–799, Oct. 2016, doi: 10.1007/978-3-662-52919-5/COVER.

[57] F. R. Menter, “Two-equation eddy-viscosity turbulence models for engineering applications,” *AIAA Journal*, vol. 32, no. 8, pp. 1598–1605, 1994, doi: 10.2514/3.12149.

[58] X. Li, L. Xu, J. Hua, X. Lin, J. Li, and M. Ouyang, “Power management strategy for vehicular-applied hybrid fuel cell/battery power system,” *J Power Sources*, vol. 191, no. 2, pp. 542–549, Jun. 2009, doi: 10.1016/j.jpowsour.2009.01.092.

[59] H. Yang, W. Zhou, L. Lu, and Z. Fang, “Optimal sizing method for stand-alone hybrid solar-wind system with LPSP technology by using genetic algorithm,” *Solar Energy*, vol. 82, no. 4, pp. 354–367, Apr. 2008, doi: 10.1016/j.solener.2007.08.005.

[60] D. Karaboga and B. Akay, “A comparative study of Artificial Bee Colony algorithm,” *Appl Math Comput*, vol. 214, no. 1, pp. 108–132, Aug. 2009, doi: 10.1016/j.amc.2009.03.090.

AUTHOR BIOGRAPHY

Author: Ms. Thuzar Mon

Degree: Master of Engineering

Date of graduation:

Date of Birth: 6th April 1997

Place of Birth: Sagaing, Myanmar

Undergraduate and Graduate Education:

Master of Engineering in Automotive Engineering,
King Mongkut's Institute of Technology Ladkrabang, Bangkok, 2023
Bachelor of Engineering in Mechanical Engineering,
Mandalay Technology University, Mandalay, 2020

Major: Automotive Engineering

Presentations and Publications:

1. T. Mon, J. Charoensuk, K. Hanamura and S. Worasinchai, "Feasibility Study of Harnessing an Urban Wind Turbine to Supply an Electric Motorbike in Thailand," 2022 International Electrical Engineering Congress (iEECON), Khon Kaen, Thailand, 2022, pp. 1-4, doi: 10.1109/iEECON53204.2022.9741568.
2. T. Mon and S. Worasinchai, "Effects of the- Rotor -C-onfiguration and the -Airfoil Shape on the Darrieus Wind Turbine Performance," 2021 13th International Conference on Information Technology and Electrical Engineering (ICITEE), Chiang Mai, Thailand, 2021, pp. 110-115, doi: 10.1109/ICITEE53064.2021.9611958.
3. T. Mon and S. Worasinchai, "Performance Modelling of the Darrieus Wind Turbine." *E3S Web of Conferences* 302:01001. doi: 10.1051/e3sconf/202130201001.